ORNL/TM-2020/1700

Full Core LOCA Safety Analysis for a PWR Containing High Burnup Fuel

Nathan Capps
Aaron Wysocki
Andrew Godfrey
Benjamin Collins
Ryan Sweet
Nicholas Brown
Soon Lee
Nicholas Szewczyk
Susan Hoxie-Key

September 30, 2020

OAK RIDGE NATIONAL LABORATORY
MANAGED BY UT-BATTELLE FOR THE US DEPARTMENT OF ENERGY

ORNL/TM-2020/1700

Reactor and Nuclear Systems Division

FULL CORE LOCA SAFETY ANALYSIS FOR A PWR CONTAINING HIGH BURNUP FUEL

Nathan Capps[1]
Aaron Wysocki[1]
Andrew Godfrey[1]
Benjamin Collins[1]
Ryan Sweet[1]
Nicholas Brown[2]
Soon Lee[2]
Nicholas Szewczyk[3]
Susan Hoxie-Key[3]

[1]Oak Ridge National Laboratory
[2]University of Tennessee, Knoxville
[3]Southern Nuclear Operating Company

Date Published: September 30, 2020

Prepared by
OAK RIDGE NATIONAL LABORATORY
Oak Ridge, TN 37831-6283
managed by
UT-BATTELLE, LLC
for the
US DEPARTMENT OF ENERGY
under contract DE-AC05-00OR22725

CONTENTS

LIST OF FIGURES v
LIST OF TABLES vi
ACRONYMS vii
ABSTRACT 1
1. INTRODUCTION 1
2. ANALYSIS TOOLS 3
   2.1 VERA 3
   2.2 RELAP5-3D 4
   2.3 BISON 4
3. ANALYSIS METHODOLOGY 4
   3.1 LOCA THERMAL HYDRAULICS 4
   3.2 FUEL PERFORMANCE 6
4. ANALYSIS RESULTS 8
   4.1 CORE DESIGN AND DEPLETION 8
      4.1.1 Reactor and Cycle Design 8
      4.1.2 Equilibrium Cycle Design Generation 10
      4.1.3 HBu10 Cycle Design Characteristics 11
   4.2 LOCA THERMAL HYDRAULICS 13
      4.2.1 Benchmark Comparison to 4-Loop Westinghouse PWR 13
      4.2.2 High Burnup LOCA Analysis 14
   4.3 FUEL PERFORMANCE 16
      4.3.1 Steady State Results 16
      4.3.2 High Burnup UO_2 Thermal Conductivity Model Comparison 25
      4.3.3 Transient Results 26
      4.3.4 Fuel Susceptibility to HBFF 30
      4.3.5 Fuel Pellet Conditions during a LOCA 32
5. CONCLUSIONS 34
6. ACKNOWLEDGMENTS 35
7. REFERENCES 35

LIST OF FIGURES

Figure 1. Generic description of Zircaloy-4 fuel rod response during a double-ended cold leg break LOCA [3]. 2
Figure 2. RELAP5-3D 4-loop Westinghouse PWR nodalization diagram. 5
Figure 3. Cladding burst criterion defined by Chapman et al. [48] for 0 ˚C/sec, 14 ˚C/sec, and 28 °C/sec. 7
Figure 4. HBFF temperature and burnup threshold developed by Turnbull et al. [49]. 8
Figure 5. The mass of the fuel susceptible to HBFF is indicated by the red rectangle. 8
Figure 6. Typical core loading strategy for a 4-loop Westinghouse PWR. 9
Figure 7. Cycle HBu10 core loading pattern. 11
Figure 8. Cycle HBu10 BOC and EOC assembly exposures (GWd/MTU) for fresh (red), once burned (green) and twice burned (blue) fuel assemblies. 11
Figure 9. Cycle HBu10 EOC fuel rod exposures (GWd/MTU). 12
Figure 10. Cycle HBu10 critical boron concentration and maximum fuel rod relative power. 12
Figure 11. Radial rod-wise power distribution at the burnup where maximum FΔH occurs. 12
Figure 12. The Vogtle FSAR and representative RELAP5-3D simulation comparisons of (a) break flow, (b) core pressure, (c) core quench front, and (d) peak cladding temperature. 14
Figure 13. The RELAP5-3D, VERA, and BISON steady-state fuel rod data integration for G8 high burnup fuel pin at the center core: (a) fuel temperature and (b) coolant and cladding surface temperatures. 15
Figure 14. (a) Fuel centerline and cladding surface temperatures, (b) heat flux, (c) heating rate at the PCT location, and (d) decay heat versus time for a LB-LOCA at EOC. 16
Figure 15. Rod average LHR for fuel rod located in Assembly G8 Pin 4-3. 17
Figure 16. Rod average LHR for fuel rod located in Assembly A11 Pin 3-13. 18
Figure 17. Rod average LHR for fuel rod located in Assembly E11 Pin 5-4. 18
Figure 18. Time-dependent RIP results for (a) G8 Pin 4-3, (b) A11 Pin 3-13, and (c) E11 Pin 5-4. 19
Figure 19. Time-dependent fuel and cladding radial strain results at the axial location 3.13 m from the bottom of the fuel for (a) G8 Pin 4-3, (b) A11 Pin 3-13, and (c) E11 Pin 5-4. 20
Figure 20. Time-dependent FGR results for (a) G8 Pin 4-3, (b) A11 Pin 3-13, and (c) E11 Pin 5-4. 21
Figure 21. Time-dependent fuel centerline temperature results at the axial location 3.13 m from the bottom of the fuel (a) G8 Pin 4-3, (b) A11 Pin 3-13, and (c) E11 Pin 5-4, indicating lower temperatures with less fission gas. 22
Figure 22. Pre-transient fuel (a) temperature profile as a function of radial position, and (b) temperature profile as a function of radial burnup at the peak power location (~3.13 m from the bottom of the active fuel). 24
Figure 23. Pretransient hoop, radial, and axial stress profile in the fuel at the peak power location of G8 Pin 4-3. 25
Figure 24. Fuel centerline temperature as a function of time 3.13 m from the bottom of the fuel stack. 26
Figure 25. End-of-life UO_2 thermal conductivity as a function of radial location across the fuel pellet. 26
Figure 26. Burst temperature as a function of burst stress for C9 Pin 7-10 (peak temperature rod). 27
Figure 27. Hoop strain and cladding temperature profile as a function of axial location at the time burst occurred for C9 Pin 7-10 (hot rod). 28
Figure 28. Experimental peak hoop strain data generated through various cladding burst test programs [10,11,63]. 29
Figure 29. Hoop strain distribution and post LOCA fuel loss measurements as a function of axial location for NRC LOCA rodlet 192 [15,16]. 29

Figure 30. Burst (a) length and (b) width correlation to the peak hoop strain observed in LOCA test programs [12–17,64,65]. 30
Figure 31. Pellet average burnup distribution at the burst location for every rod that exceeded a rod average burnup of 62 GWd/MTU. 30
Figure 32. Percentage of fuel pellet susceptible to pulverization in percent for the best estimate and core-wide PCT over the burnup range of interest. 31
Figure 33. Radial temperature evolution of prior to and during LOCA. 32
Figure 34. Radial (a) hoop stress, (b) radial stress, and (c) axial stress evolution prior to and during LOCA. 33

LIST OF TABLES

Table 1. Transition and equilibrium 24-month cycle design information. 10
Table 2. Comparison of Utility Simulation and VERA results for equilibrium 24-month cycle design. 13
Table 3. Steady-state rod average peaking factor, PCT, and local burnup at PCT location for considered fuel rods. 16
Table 4. Full core estimation of HBFF susceptibility 32

ACRONYMS

AIC	silver-indium-cadmium
ANS	American Nuclear Society
AOO	anticipated operation occurrences
BOC	beginning of cycle
CASL	Consortium for Advanced Simulation of Light Water Reactors
CFR	US Code of Federal Regulations
DBA	design basis accident
DOE	US Department of Energy
ECCS	emergency core cooling system
EFPD	effective full power day
EOC	end of cycle
FFRD	fuel fragmentation, relocation, and dispersion
FGR	fission gas release
FSAR	final safety analysis report
HBFF	high-burnup fuel fragmentation
IFA	instrumented fuel assembly
IFBA	integral fuel burnable absorber
INL	Idaho National Laboratory
LB-LOCA	large-break LOCA
LEU	low-enriched uranium
LHR	linear heat rating
LOCA	loss-of-coolant accident
LWR	light-water reactor
MOC	method of characteristics
MOOSE	Multiphysics Object-Oriented Simulation Environment
NEAMS	Nuclear Energy Advanced Modeling and Simulation Program
NFIR	Nuclear Fuel Industry Research
NPP	nuclear power plant
NRC	US Nuclear Regulatory Commission
PCT	peak cladding temperature
PWR	pressurized water reactor
RCCA	rod control cluster assembly
RCS	reactor coolant system
RELAP5-3D	Reactor Excursion and Leak Analysis Program
RFA	robust fuel assembly
RIP	rod internal pressure
RPV	reactor primary vessel
SCIP	Studsvik Cladding Integrity Project
SNC	Southern Nuclear Operating Company
TEDE	total effective dose equivalent
TREAT	Transient Reactor Test Facility
WABA	wet annular burnable absorber

ABSTRACT

High burnup fuel fragmentation, relocation, and dispersal is one of the largest hurdles for the nuclear industry to clear before rod average burnup can be increased beyond 62 GWd/MTU. This objective of this work is to inform the high burnup loss-of-coolant-accident (LOCA) safety case for a core containing high burnup fuel to help accelerate the nuclear industry's goals to (1) extend cycle lengths to 24 months and (2) increase peak rod average burnup to 75 GWd/MTU. The results of this analysis will define realistic, prototypic LOCA conditions to design subsequent separate effects and integral testing and will inform advanced modeling and simulation to develop mechanistic models. US Department of Energy tools were used to evaluate commercial pressurized water reactor (PWR) fuel susceptible to fragmentation under high burnup conditions. Realistic, rather than bounding, 24-month core designs and operating conditions (power history, axial profile, thermal boundary condition, flux, etc.) for VERA depletion analyses were provided by an industry partner. RELAP5-3D provided LOCA transient conditions (decay heat, thermal hydraulic conditions, etc.) for a core containing high burnup fuel (i.e., over 62 GWd/MTU with peak rod being 75 GWd/MTU). These operating conditions were entered into BISON to evaluate the evolution of the high burnup fuel under steady-state and transient conditions. BISON was used to determine the limiting fuel rod in each high burnup assembly and to evaluate the impact of pretransient fuel conditions (i.e., radial temperature profile), clad strain, ballooning behavior, and burst timing on the fuel's susceptibility to high burnup fuel fragmentation. These efforts culminated in this summary of the potential impacts of high burnup fuel fragmentation, relocation, and dispersal and definition of prototypic LOCA conditions.

1. INTRODUCTION

For economic reasons, the US nuclear industry is renewing efforts to build a technical basis to extend peak rod average burnup limits above the current regulatory burnup limit of 62 GWd/MTU [1]. The primary driver of these efforts is to economically increase pressurized water reactor (PWR) cycle lengths to 24 months, reduce the number of fresh fuel assemblies, increase time online, thereby reducing number of outages and their associated cost, higher fuel utilization, and possibly reduce core design constraints. In order for US nuclear utilities to leverage these economic efficiencies, the US Nuclear Regulatory Commission (NRC) will likely require nuclear power plants (NPPs) to analyze a number of potential operational occurrences and their potential consequences with each new core design prior to resuming normal operation [1]. Potential operational occurrences can be divided into three primary regimes: (1) normal operation, (2) anticipated operation occurrences (AOOs), and (3) design basis accidents (DBAs). Normal plant operation is an operating regime in which the plant operates within specified operational limits until the end of the cycle, whereas AOOs are events that result in the NPP deviating outside the normal operating regime. A key attribute of an AOO is that the occurrence should be expected. However, by definition, the occurrence of an AOO does not result in significant impact to critical safety functions. The last potential operational occurrence is a DBA. From the fuel performance point-of-view, DBAs can be subdivided into two bounding categories: (1) loss of coolant accidents (LOCAs), and (2) reactivity insertion accidents (RIAs). Unlike AOOs, DBAs may result in fuel rod failure. The NRC imposes fundamental acceptance criteria to minimize radiological consequences to the public and onsite staff. Furthermore, safety criteria are typically linked to the fulfillment of other acceptance criteria related to reactor safety equipment designed to mitigate DBAs.

A LOCA is one of the most important postulated accident scenarios for light-water reactors (LWRs). A LOCA occurs when the primary coolant system suffers a failure resulting in the loss of reactor coolant. The most severe (and least probable) accident initiating event is a double-ended guillotine break between the reactor vessel and the main circulation pump. An example of a PWR fuel rod response during a double-ended guillotine break is illustrated in Figure 1 [3]. Following rupture of the cold legs, the coolant

flashes to steam and blows down through the ruptured pipes. Fission product decay heat continues to heat the fuel and reactor internals in the wake of coolant loss. This further supports the need to establish long-term cooling to mitigate such accident consequences. Reactor depressurization is completed within ~20–30 seconds into the transient. Once depressurized, the emergency core cooling system (ECCS) begins pumping water into the reactor primary vessel (RPV). Initially, the ECCS is unable to provide sufficient cooling to the fuel elements, and during this time, decay heat continues to increase fuel rod temperatures [3] to the point at which permanent fuel damage may occur, including ballooning, burst, and ultimately, oxidation and hydriding, resulting in the loss of post quench ductility [4]. The severity of the LOCA transient is governed by a number of conditions related to the local fuel rod and assembly.

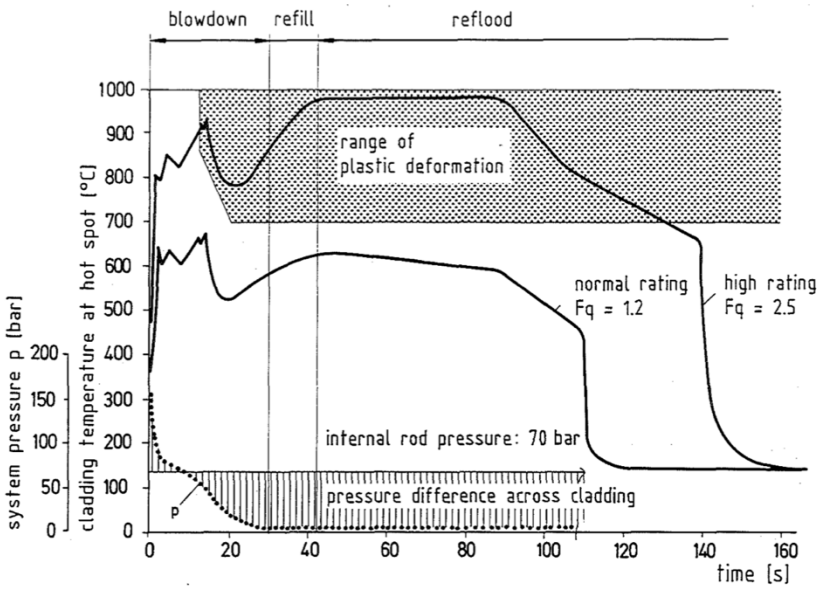

Figure 1. Generic description of Zircaloy-4 fuel rod response during a double-ended cold leg break LOCA [3].

In the early- to mid-2000s, high burnup LOCA experiments performed at the Halden Boiling Water test reactor indicated that high burnup fuel, >80 GWd/MTU, was susceptible to fuel pellet fragmentation and pulverization, termed *high burnup fuel fragmentation* (HBFF), in which parts of the fuel pellet fragmented into an effective sand like consistency, with fuel particles less than 1 mm [8–10]. Subsequently, pulverized fuel could relocate into the balloon region, and following burst, it could disperse from the cladding. The issue gained attention when HBFF was observed to be closer to the current US regulatory limit (62 GWd/MTU) during NRC-sponsored out-of-core integral testing at Studsvik Nuclear in early 2011 [11,12]. The experimental results identified a burnup range between 65 and 72 GWd/MTU, at which fuel pellets begin to pulverize and become susceptible to relocation and dispersion. The Studsvik test results led to NRC concerns regarding potential changes to fuel and core designs that could result in HBFF. Subsequent HBFF research has come to similar conclusions [8–19].

Analyses have been performed to evaluate integral and semi-integral rod burst experiments, as well as more complicated integral experiments performed at Halden and Studsvik [20–24]. However, these analyses were focused on evaluating the impact of various packing fractions in order to evaluate the impact of fuel relocation on peak cladding temperature (PCT). In 2018, a round robin study was conducted as a part of the Studsvik Cladding Integrity Project (SCIP) III program [24]. The study evaluated the porosity, fission gas distribution, balloon burst criteria, and cladding strain for SCIP III LOCA experiments. Work performed at Idaho National Laboratory (INL) demonstrated BISON's capability to model fuel relocation [25], and furthermore, an exhaustive overview of the LOCA capabilities in BISON was well documented [26]. In an effort to begin evaluating high burnup effects at

the core level, H. Zhang evaluated five high burnup core designs based on the South Texas Nuclear Power Plant in order to evaluate cladding burst potential at higher burnups [27]. To date, these analyses have not begun to address the NRC concerns related to fuel fragmentation and its potential to be dispersed from the fuel rod; nor have they begun to inform the industry's high burnup LOCA safety case. Therefore, a modern approach is needed to holistically evaluate the response of high burnup fuel under LOCA conditions

This project used a fully integrated approach by externally coupling VERA, RELAP5-3D, and BISON to evaluate HBFF susceptibility for a 4-loop high powered Westinghouse PWR. Southern Nuclear Operating Company (SNC) developed representative core designs to support a simulation for the transition from 18- to 24-month cycles. Depletion of these core designs in VERA provided the necessary input to RELAP5-3D to evaluate thermal and pressure response of the system. Lastly, VERA and RELAP5-3D results provided BISON with the necessary boundary conditions to evaluate the evolution of high burnup fuel under steady-state and LOCA conditions in order to calculate the total mass in the core that would be susceptible to HBFF. Demonstration of these capabilities helps to inform the US nuclear industry's high burnup LOCA safety case by calculating a conservative value for mass susceptible to HBFF to support subsequent accident consequence analysis. Furthermore, this evaluation can serve as a benchmark problem for fuel suppliers, utilities, and research organizations to which they can compare the results of their codes. The full core LOCA results can be used to develop targeted separate effects testing designed to evaluate HBFF relocation and dispersal. Separate effects test results can be used to validate and refine the full core high burnup LOCA results and to support justification for large-scale integral high burnup LOCA testing at INL's Transient Reactor Test Facility (TREAT).

2. ANALYSIS TOOLS

2.1 VERA

VERA is a state-of-the-art reactor analysis suite of high-fidelity software and methods capable of simulating the full operating history of a commercial PWR [28]. It includes advanced solvers and multiphysics coupling algorithms. VERA can accurately calculate fuel rod and coolant conditions at very small spatial scales, including time-dependent isotopic depletion and decay, burnable poison depletion, and in-core detector response. VERA can also simulate local impacts of control rod movement and explicit effects of fuel assembly decay and shuffling during refueling outages. VERA has been applied to nearly ⅔ of the US commercial PWRs for simulation of over 200 operating fuel cycles [28,29-32].

The methods employed by VERA for steady-state core follow analyses are described below. While VERA has a variety of other capabilities—including fuel rod performance, simulations of CRUD and corrosion growth in the PWR primary coolant system, and transient reactivity insertion accident analyses—the most prominent and mature capability in VERA is the simulation of nominal reactor operation. The dominant components of VERA used in this work are detailed below:

- **MPACT**: An advanced pin-resolved whole-core multigroup deterministic neutron transport capability based on the 2D/1D synthesis method on the frame of a 3D coarse mesh finite difference method, for which radial and axial correction factors are obtained from 2D method-of-characteristics (MOC) and 1D P_N, respectively [32]. MPACT uses a 51 energy-group cross section library based on ENDF/B-VII.1 data and the subgroup method of on-the-fly resonance self-shielding [33] to obtain accurate neutron reaction rates at precise local conditions anywhere in the reactor core. MPACT has been extensively validated against a variety of critical experiments and results from continuous-energy Monte Carlo–based methods.

- **CTF**: An advanced subchannel thermal-hydraulics capability using a transient two-fluid, three-field (i.e., liquid film, liquid drops, and vapor) modeling approach to determine the thermodynamic conditions in every coolant subchannel in the reactor core, including cross-flow effects from turbulent mixing and lateral pressure gradients [34]. CTF has been validated against a broad array of single- and two-phase tests for the assessment of prediction of void generation, mixing, heat transfer, pressure drop, fuel rod behavior, and droplet entrainment in a variety of different geometries.

- **ORIGEN**: An isotopic depletion and decay code capable of characterizing used fuel (including activity, decay heat, radiation emission rates, and radiotoxicity), generating source terms for accident analyses, and activating structural materials [35]. The application programming interface enables a direct coupling to MPACT for simulation of fuel depletion and decay in millions of unique depletion regions in a reactor core. ORIGEN has been widely used and validated over the last four decades as part of the SCALE code suite [36].

2.2 RELAP5-3D

The Reactor Excursion and Leak Analysis Program (RELAP5-3D) was developed at INL to model various operational transients and postulated accidents in LWR systems [46]. RELAP5-3D is a systems code for analyzing thermal-hydraulic response of core and reactor coolant system (RCS) during various transients, including both small- and large-break LOCAs (LB-LOCAs). The RELAP5-3D solves two-fluid system using partially implicit numerical scheme based on a nonhomogeneous and nonequilibrium model. The code consists of various generic component models including pumps, valves, pipes, heat exchange structures, reactor kinetics, heaters, turbines, compressors, pressurizers, accumulators, and control system components. It is capable of modeling effects such as form loss, flow at an abrupt area change, branching, choked flow, boron tracking, non-condensable gas transport, two-phase flow dynamics, pre- and post-CHF heat transfer, and quench front tracking. In this study, RELAP5-3D is used to perform LB-LOCA analysis on a 4-loop Westinghouse PWR to provide systems response and transient temperature behavior of high burnup fuel to BISON.

2.3 BISON

BISON is a fuel performance code built upon the Multiphysics Object-Oriented Simulation Environment (MOOSE) developed at INL [37]. MOOSE is a parallel finite element computational system that uses a Jacobian-free, Newton-Krylov method to solve coupled systems of nonlinear partial differential equations. The MOOSE framework provides the ability to effectively use the massively parallel computational capabilities that are needed to create high-fidelity 3D fuel rod, full-length R-Z rod, and R-θ geometric representations [38].

3. ANALYSIS METHODOLOGY

3.1 LOCA THERMAL HYDRAULICS

System-level best-estimate transient simulations are conducted to evaluate susceptibility of fuel pellet fragmentation and pulverization in high burnup fuel under LB-LOCA conditions. A typical 4-loop Westinghouse PWR plant with a rated power of 3,626 MW is constructed using RELAP5-3D with generic 1D components, which consists of the main reactor features governing system response under the reference scenario. A generic 4-loop Westinghouse PWR RELAP5-3D model was established based on a legacy Zion model (typpwr.i). The system consists of reactor core vessel and internal components, intact and broken loops with hot and cold legs, primary coolant pumps, steam generators, pressurizer, and the ECCS (see Figure 3). The secondary loop connected with the steam generator is modeled with main feedwater and auxiliary feedwater volumes controlling water injection boundary conditions, and with the

main steam safety valves and pilot operated relief valves governing the secondary system pressure to attain desired steady-state primary coolant temperature.

For practicality, homogenized reactor core simulations are used to reduce the number of flow channels and rods. The reactor core is simulated with two pipe fuel channels connected with cross-flow junctions comprised of fifty axial nodes, implementing identical axial nodalization from VERA. The main core channel represented the average fuel rod (component number 336), and the other represented the single subchannel surrounding the rod of interest (component number 337), as the intent was to evaluate the high burnup fuel rod system response during the transient. Separate runs were conducted on four selected rods of interest. The rods were high burnup and peak temperature rods selected from various core regions. Heat structures representing fuel rods in each channel were comprised of fifty nonuniform axial nodes to capture the axial power distribution and to match the BISON meshing scheme.

Figure 2 illustrates a simplified representation of the 4-loop Westinghouse PWR LB-LOCA model. In this study, LB-LOCA only considered a cold-leg double-ended guillotine break, as illustrated in Figure 2 components 212, 214, and 500. It is considered the most limiting LOCA scenario, as it limits ECCS injection from the cold-leg, promotes flow stagnation, and causes ECCS injection bypass. Pressure drop caused from the break initiates primary and secondary sides to trip. When the accumulator set pressure is reached, the accumulator starts injecting coolant into the primary loop. Emergency generators are initiated to operate high-pressure injection systems after a short delay. Then the low-pressure injection systems are operated to inject coolant into the reactor core to fully quench the core vessel. LB-LOCAs consist of blowdown, refill, reflood, and long-term cooling phases, all of which are modeled. HBFF susceptibility evaluations under the most limiting LOCA scenario were carried out.

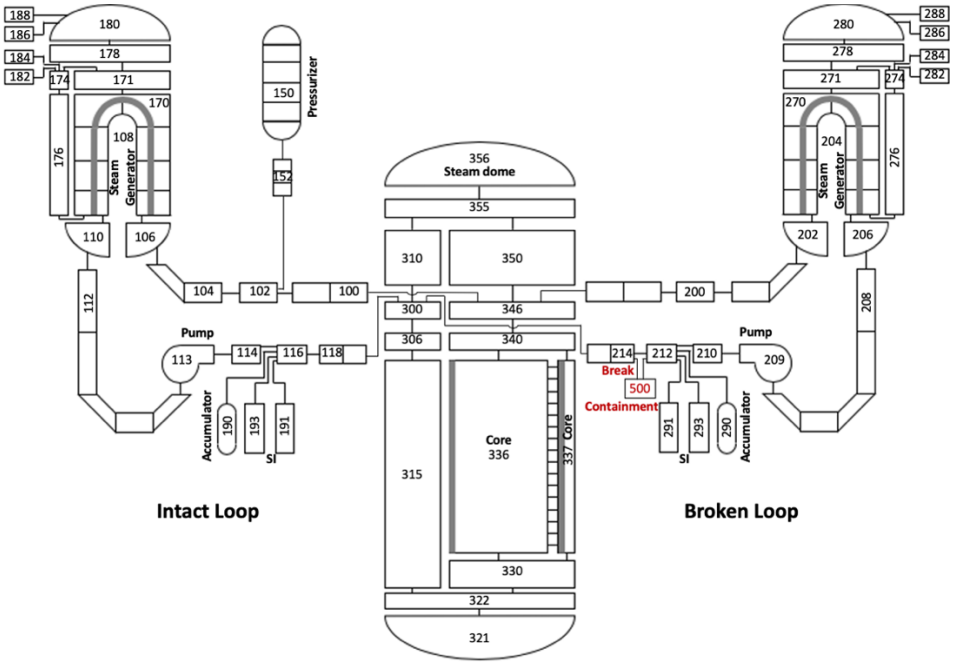

Figure 2. RELAP5-3D 4-loop Westinghouse PWR nodalization diagram.

The RELAP5-3D LB-LOCA model was established and compared to the LB-LOCA results in the final safety analysis report (FSAR) to ensure realistic thermal and pressure responses [39]. Because the RELAP5-3D model was developed based on a Westinghouse 4-loop PWR design (Zion), the plant configuration is largely consistent with the plant reported in the FSAR. Furthermore, core geometry and operating conditions were applied in the RELAP5-3D model consistent with the high-burnup cycle

design, as described below. For comparison, the nominal cycle design described in the FSAR, including peaking factor and fresh fuel thermal properties, was applied to the RELAP5-3D model. Therefore, reasonable agreement was expected between the two sets of results, and a comparison was performed to ensure that RELAP5-3D results were consistent with the reported LB-LOCA behavior. For this comparison, the built-in point kinetics model used reference peaking factors from the American Nuclear Society (ANS) Appendix K decay heat standard [40].

The following four fuel pins from different assemblies were selected based on the end-of-cycle (EOC) burnup level and core location. Assembly A11 pin 3-13 has the highest rod average burnup (75.8 GWd/MTU) on the core periphery. Assembly C9 pin 7-10 is the hottest rod, with an average burnup of 38.9 GWd/MTU. Assembly E11 pin 5-4 represents the average pin power with an average burnup of 67.7 GWd/MTU. Assembly G8 pin 4-13 represents high burnup fuel (70.5 GWd/MTU) in the central regions of the core.

The steady-state power profile, the cladding surface temperature, subchannel coolant temperature, and pressure data from the MPACT and CTF calculations were implemented in the RELAP5-3D hot channel to match pretransient conditions. Based on VERA data, BISON generated the following burnup-dependent parameters for each fuel rod at EOC: rod internal pressure, number of fission gas moles, radial displacement, and pellet-cladding gap thickness. RELAP5-3D used the BISON results to inform the gap conductance model and fuel cladding deformation model to accurately calculate gap thickness, gap thermal conductivity, and pretransient fuel temperature. Subsequently, RELAP5-3D was compared to BISON to ensure that the pretransient fuel rod conditions were identical between the two codes. The Nuclear Fuel Industry Research (NFIR) correlation was used to calculate temperature dependent fuel thermal conductivity using the average fuel rod burnup [41]. Cladding thermal properties used the cladding models documented in MATPRO [42].

3.2 FUEL PERFORMANCE

Fuel rod evolution under steady-state and transient conditions is critical for evaluating fuel susceptibility to HBFF. Steady-state irradiation conditions prior to the transient impacts fuel rod conditions governing the fuel rod performance during LOCA. For example, clad ballooning is governed by rod internal pressure and temperature. However, rod internal pressure is governed by cladding creep down, fuel swelling, relocation, thermal expansion, fission gas release, etc., all of which differ under various operating conditions. To capture prototypic conditions, SNC developed representative core designs to support a simulation of a 4-loop Westinghouse PWR for implementation into VERA for cycle depletion. VERA depletion results provided steady-state operating conditions at the level of the assembly and the fuel rod for subsequent thermal hydraulic and fuel performance modeling.

Calculating fuel susceptibility to HBFF was more complicated. First, time-dependent and spatially dependent fuel rod decay and thermal hydraulic boundary conditions were needed to model the LOCA transient. Time-dependent and spatially dependent decay heat profiles were calculated in VERA immediately following reactor scram for a specified period of time (approximately one hour or longer if needed). RELAP5-3D used the VERA steady-state and decay heat results to evaluate the system temperature and pressure response on the fuel rod and assembly level. VERA and RELAP5-3D results served as input and boundary conditions for BISON to calculate fuel susceptibility to HBFF. However, to calculate fuel susceptibility to HBFF, a number of criteria or thresholds were needed to evaluate the performance of the fuel throughout the LOCA.

The methodology outlined by Capps et al. [43] was used to calculate fuel susceptibility to HBFF. The methodology first determines when or if burst occurs. Burst is determined by using the criterion developed by Chapman et al. [44], as shown in Eq. (1). Figure 3 illustrates the burst criterion as defined

by the equation for three different heating rates (0°C/sec, 14°C/sec, and 28°C/sec). The cladding heating rate must be evaluated to determine which curve is most appropriate to use for each fuel rod. This could impact the timing of burst, as well as clad balloon behavior. Work performed at INL [27] indicates that the heating rate changes as a function of time, with the initial heating rate ranging from ~24–34 °C/sec, and then it decreases to ~2–5°C/sec. Therefore, each rod must be independently evaluated Then the cladding hoop strain in the vicinity of the burst location was evaluated. Integral LOCA experiments performed at Studsvik and sponsored by the NRC indicate that the cladding can constrain HBFF. The experimental results [11] show that a cladding hoop strain of 4% at the top of the balloon will prevent HBFF, whereas the bottom of the balloon can strain to 5–6%. For the purposes of this analysis, a 4% hoop strain threshold was applied to the upper regions of the balloon, and a 5% hoop strain threshold was applied to the lower region of the balloon. This threshold requires that the cladding exceed the specified strain value in order for the fuel to become susceptible to HBFF. However, if the cladding does not exceed the threshold, then the fuel will be adequately restrained and not susceptible to HBFF. The fuel where the cladding exceeded the strain threshold was evaluated and compared to the HBFF threshold illustrated in Figure 4. The fuel in the susceptible region was assessed on a nodal burnup and temperature level throughout the susceptible region. There may be regions of the fuel, specifically at the center of the fuel, where the local burnup and temperature are above the HBFF threshold. If this were to occur, then it would be assumed that the fuel was susceptible to HBFF if the local (i.e., nodal) temperature increased; if the local fuel temperature decreased or remained the same, then the fuel would not be considered susceptible to HBFF. Figure 5 illustrates how each criterion was being applied on a rod-by-rod basis to assess HBFF susceptibility.

$$T_R = 3960 - \frac{2.96\sigma}{1-H} - \frac{1.23 \times 10^6 \sigma}{100(1+H) + 405\sigma} \quad (1)$$

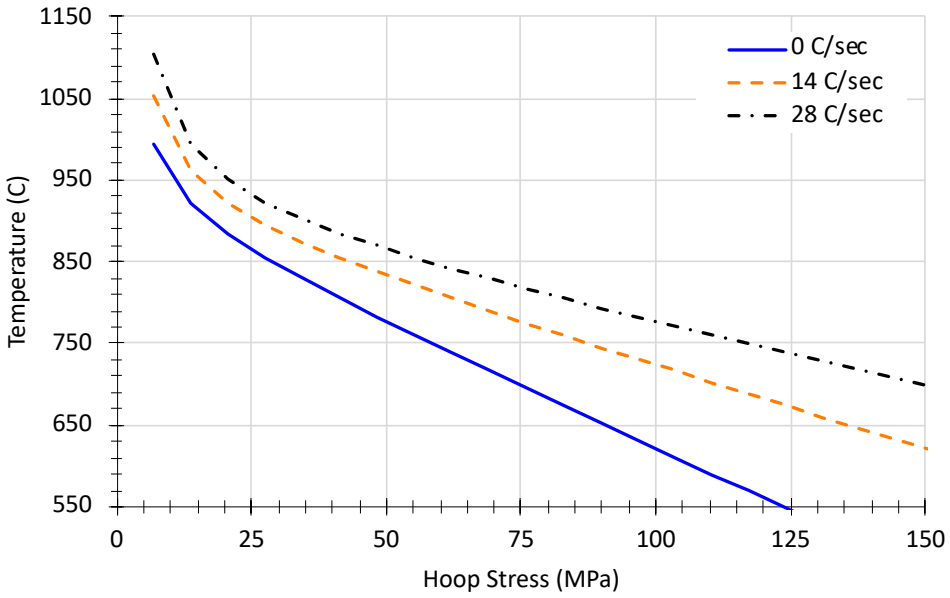

Figure 3. Cladding burst criterion defined by Chapman et al. [44] for 0 °C/sec, 14 °C/sec, and 28 °C/sec.

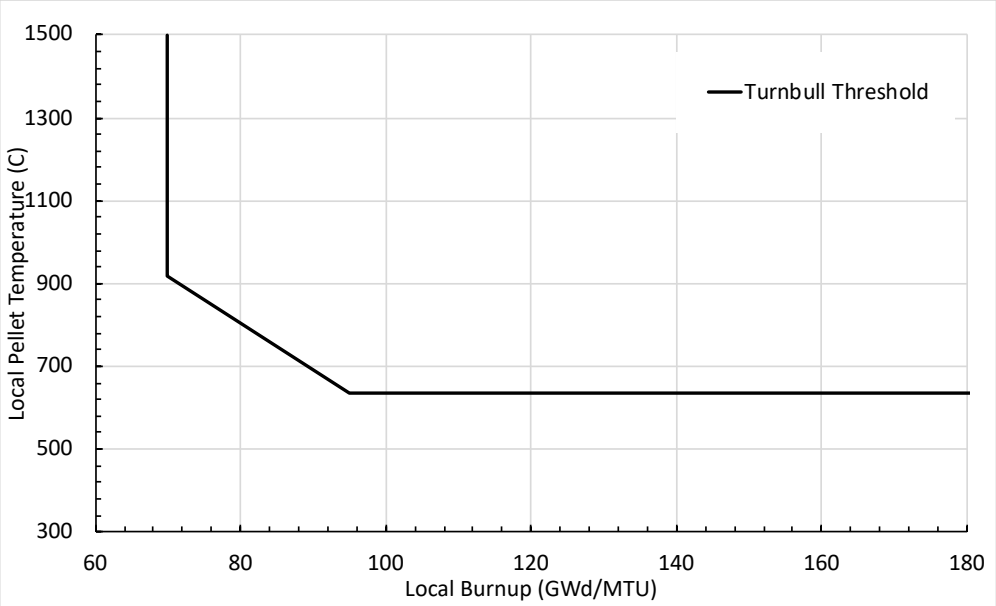

Figure 4. HBFF temperature and burnup threshold developed by Turnbull et al. [45].

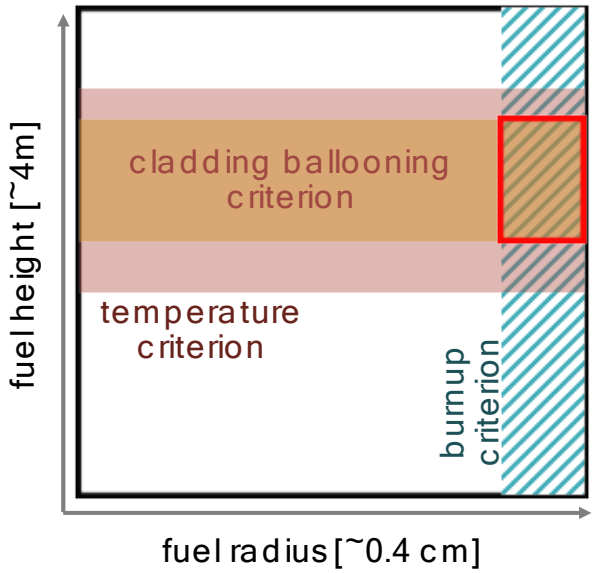

Figure 5. The mass of the fuel susceptible to HBFF is indicated by the red rectangle. In this region, all three criteria for cladding constraint, fuel temperature, and local burnup exceed their limits [43].

4. ANALYSIS RESULTS

4.1 CORE DESIGN AND DEPLETION

4.1.1 Reactor and Cycle Design

The Westinghouse four-loop commercial PWR used for this analysis is an ambient pressure containment design with a capacity of 193 nuclear fuel assemblies and a rated power of 3,626 MW_{th}. Current fuel management strategies employ 18-month fuel cycle designs with a typical low-leakage "ring-of-fire" fresh fuel layout using low-enriched uranium (LEU) fuel. Three burnup regions are typically used. 85–92

17×17 fresh fuel assemblies are checkerboarded with once-burned assemblies in the core interior and used in a "ring of fire" one row interior to the core periphery. The core periphery consists of once- and twice-burned assemblies. See Figure 6. Cycles are designed to operate continuously for approximately 500 effective full power days (EFPD). Combinations of integral fuel burnable absorber (IFBA) and wet annular burnable absorber (WABA) types are used in fresh fuel assemblies to optimize power distributions and to reduce the amount of soluble boron in the reactor coolant, which is used for excess reactivity control. Silver-indium-cadmium (AIC) rod control cluster assemblies (RCCAs) are typically used for power regulating and safety functions.

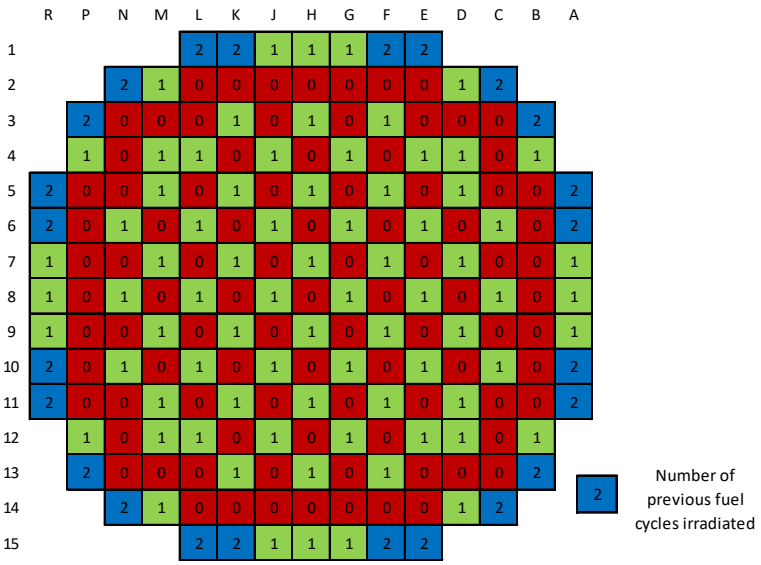

Figure 6. Typical core loading strategy for a 4-loop Westinghouse PWR.

The process to develop a 24-month fuel cycle design used high-enrichment and high-burnup fuel built on previous core designs and depletion results. SNC developed representative loading patterns and optimization based upon their familiarity with 4-loop PWR cores and core designs. To meet all design criteria, a transition was performed from a previous core design used in a 4-loop PWR. Two cycles were transitioned from 18- to 24-month designs. In reality, it would likely take utilities additional cycles to transition to 24-month core designs, as additional fuel management and licensing concerns may prevent rapid transitions. Each of the 24-month core designs was intended to be realistic, rather than bounding all possible core designs. Ten additional 24-month core designs were developed to reach an equilibrium pattern. Representative core design results developed by Southern were compared to VERA results to ensure consistency. Design criteria employed by Southern Nuclear included:

- Fuel enrichments less than 6.95 wt% ^{235}U (beyond the current 4.95 wt% limit)
- Peak fuel rod exposure of ~75 GWd/MTU (beyond the current 62 GWd/MTU limit)
- Approximately 700 EFPD design cycle length
- Minimal number of once-burned fuel on the core periphery
- Approximately 84 fresh feed assemblies per cycle
- Typical low-leakage in/out ring-of-fire loading pattern
- $F\Delta h$ limit of 1.50 (similar to existing 18-month cycle designs)
- IFBA/WABA only for burnable poisons (no gadolinia)
- Fresh center assembly every other cycle

The design strategy incorporated a common technique of loading a single fresh assembly into the center of the reactor core and leaving it there for two cycles. The advantages of this strategy are that the fuel is better utilized, and fuel rod burnups are minimized in the center assembly location as opposed to breaking up symmetric assemblies for that location. However, one drawback of this approach is that twice as many cycles are needed to reach equilibrium designs. Thus, the target 24-month cycle equilibrium design is actually a pair of cycles. For this work, the cycle that was the most limiting in power and burnup was selected for downstream analysis.

To achieve 24-month cycle lengths, the fuel type was changed to a slightly "fatter" (i.e. larger diameter) fuel rod design to accommodate ~9% more fuel. Another difference included using a slighter shorter intermediate spacer grid with a reduced form loss coefficient. This fuel transition was implemented during the first transition cycle and beyond with the inclusion of increased enrichment.

4.1.2 Equilibrium Cycle Design Generation

Representative transition and high burnup core designs were developed by Southern Nuclear Operating Company (SNC) to provide realistic and feasible patterns based on current reload design and safety analysis constraints. In the future, more detailed analyses may reveal some problematic characteristics such as high boron concentration, CIPS susceptibility low shutdown margin, and adding RCCAs and control rod drive mechanism in spare slots, but these were not considered for this analysis. The primary goal for this work was to generate power histories for high-enrichment, high-burnup fuel for subsequent LOCA and FFRD analysis. Table 1 provides cycle design information relating to the loading pattern generation. Note that the design strategy for the center assembly resulted in pairs of equilibrium cycles, and Table 1 core designs do not represent the actual designs in operation. Cycle HBu10 was selected as the equilibrium pattern for further analysis.

Table 1. Transition and equilibrium 24-month cycle design information.

Cycle	Cycle length (EFPD)	Number of feeds	Feed enrichments (wt% ^{235}U)	Number IFBA/WABA	Maximum fuel rod FΔh	Maximum fuel rod burnup (GWd/MTU)
T1[*]	522.7	92	4.60/4.95/5.20	11616/400	1.46	56.1
T2[-]	695.1	93	5.20/5.60/5.95	16024/784	1.48	61.6
HBu1[+]	700	92	5.60/5.95/6.20	16480/848	1.47	70.2
HBu2	693	89	5.60/5.95/6.20	16072/736	1.46	70.5
HBu3	693	84	5.95/6.20/6.60	16096/592	1.49	73.1
HBu4	693	81	5.95/6.20/6.60	15128/592	1.49	73.1
HBu5	693	84	5.95/6.20/6.60	16032/624	1.50	78.1
HBu6	693	85	5.95/6.20/6.60	16056/704	1.49	75.5
HBu7	693	84	5.95/6.20/6.60	16032/608	1.49	73.3
HBu8	693	85	5.95/6.20/6.60	16056/704	1.50	76.8
HBu9	693	84	5.95/6.20/6.60	16032/608	1.49	74.3
HBu10	**693**	**85**	**5.95/6.20/6.60**	**16056/704**	**1.50**	**76.9**
HBu11	693	84	5.95/6.20/6.60	16032/608	1.49	74.3
HBu12	693	85	5.95/6.20/6.60	16056/704	1.50	75.9

[*] *T indicates 18 to 24-month transition cycles*
[+] *HBu indicates 24-month cycles with increased enrichment and burnup*
[-] T2 is a transition cycle and includes high burnup fuel

4.1.3 HBu10 Cycle Design Characteristics

Cycle HBu10 achieved a 693 EFPD cycle length and a peak fuel rod average burnup of 76.9 GWd/MTU. The core loading pattern for the equilibrium cycle is shown in Figure 7 in quarter-core symmetry, with enrichment and burnable poisons provided for the feed fuel, and previous cycle locations provided for the reinsert fuel. VERA-calculated BOC and EOC peak pin burnups are provided in Figure 8, and the rod-wise burnup distribution is provided in Figure 9. Figure 10 provides the critical boron letdown for the equilibrium cycle, as well as the maximum fuel rod relative power (FΔH). Figure 11 displays the radial rod-wise power distribution from VERA at the burnup where it reaches the maximum FΔH. Lastly, VERA Cycle HBu10 results were compared to the methods used by Southern Nuclear to ensure consistency between several parameters of interest. The comparison is shown in Table 2 and demonstrates remarkable agreement considering the large difference between the two models and methods.

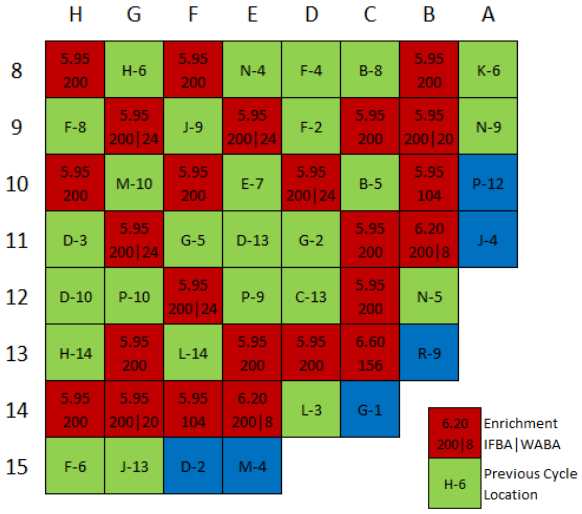

Figure 7. Cycle HBu10 core loading pattern.

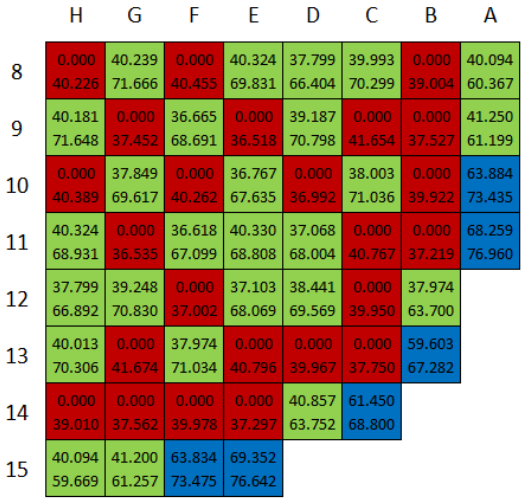

Figure 8. Cycle HBu10 BOC and EOC peak pin exposures (GWd/MTU) for fresh (red), once burned (green) and twice burned (blue) fuel assemblies.

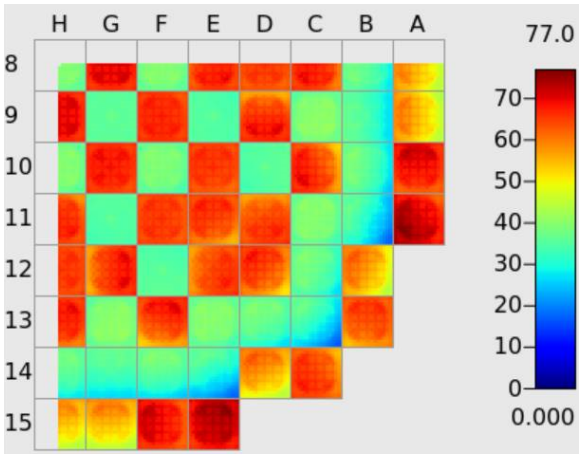

Figure 9. Cycle HBu10 EOC fuel rod exposures (GWd/MTU).

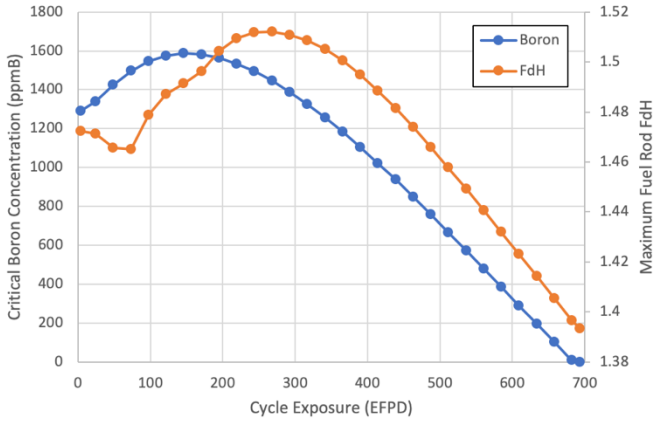

Figure 10. Cycle HBu10 critical boron concentration and maximum fuel rod relative power.

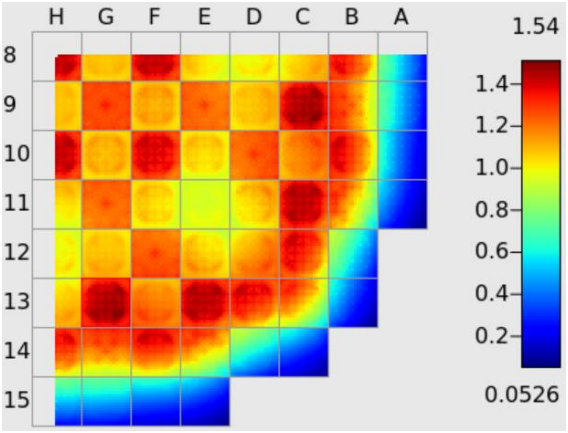

Figure 11. Radial rod-wise power distribution at the burnup where maximum FΔH occurs.

Table 2. Comparison of Utility Simulation and VERA results for equilibrium 24-month cycle design.

Parameter	Utility Simulation	VERA	Percent difference (%)
Maximum fuel rod power	1.49	1.51	0.8
Maximum local pin power	1.76	1.85	5.3
Maximum assembly power	1.39	1.39	0.0
Maximum fuel rod burnup	76.8	76.9	0.1
Maximum boron concentration	1568	1586	0.01

4.2 LOCA THERMAL HYDRAULICS

4.2.1 Benchmark Comparison to 4-Loop Westinghouse PWR

We conducted an assessment of our 4-Loop Westinghouse PWR model to ensure that our baseline results were in good agreement with the PWR FSAR. The PWR FSAR system parameters, including the rated power, peaking factor, and accumulator and pressurizer set points, were implemented in the model for a consistent comparison. A parametric study of four discharge coefficients (0.4, 0.6, 0.8, and 1.0) was conducted to investigate break flow and pressure drop trends over the coefficients. Both break flow and pressure drop from the RELAP5-3D model showed comparable behavior to the FSAR results. The most limiting case of 1.0 discharge coefficient is considered in this study. The model's overall break flow and pressure drop responses are in good agreement with the results reported in the FSAR, shown in Figure 12 (a). A slight discrepancy in the break flows during the blowdown phase can be observed during the time from 0 to 2.5 seconds. which triggered a delay in the core pressure drop as shown in Figure 12 (b). This is due to the minor differences between the model and the FSAR results in pre-transient steady-state operating temperatures (~25°C) and break loop flow (~500 kg/s). The core quench front of the model is shown in Figure 12 (c), which showed more conservative results in the present model compared to the response in the FSAR. Figure 12 (d) shows the cladding temperature response at the peak cladding temperature (PCT) location during the LB-LOCA. The PCT was reached at 200 seconds and 250 seconds for PWR FSAR and the present RELAP5-3D model, respectively. The discrepancy in the applicable time of PCT occurred due to the difference in the aforementioned pre-transient conditions and the system response during the blowdown, refill, and reflood. The PCT responses showed good agreement. The reported PCTs were 1029°C and 1023°C for RELAP5-3D and the PWR FSAR, respectively, as shown in Figure 12.

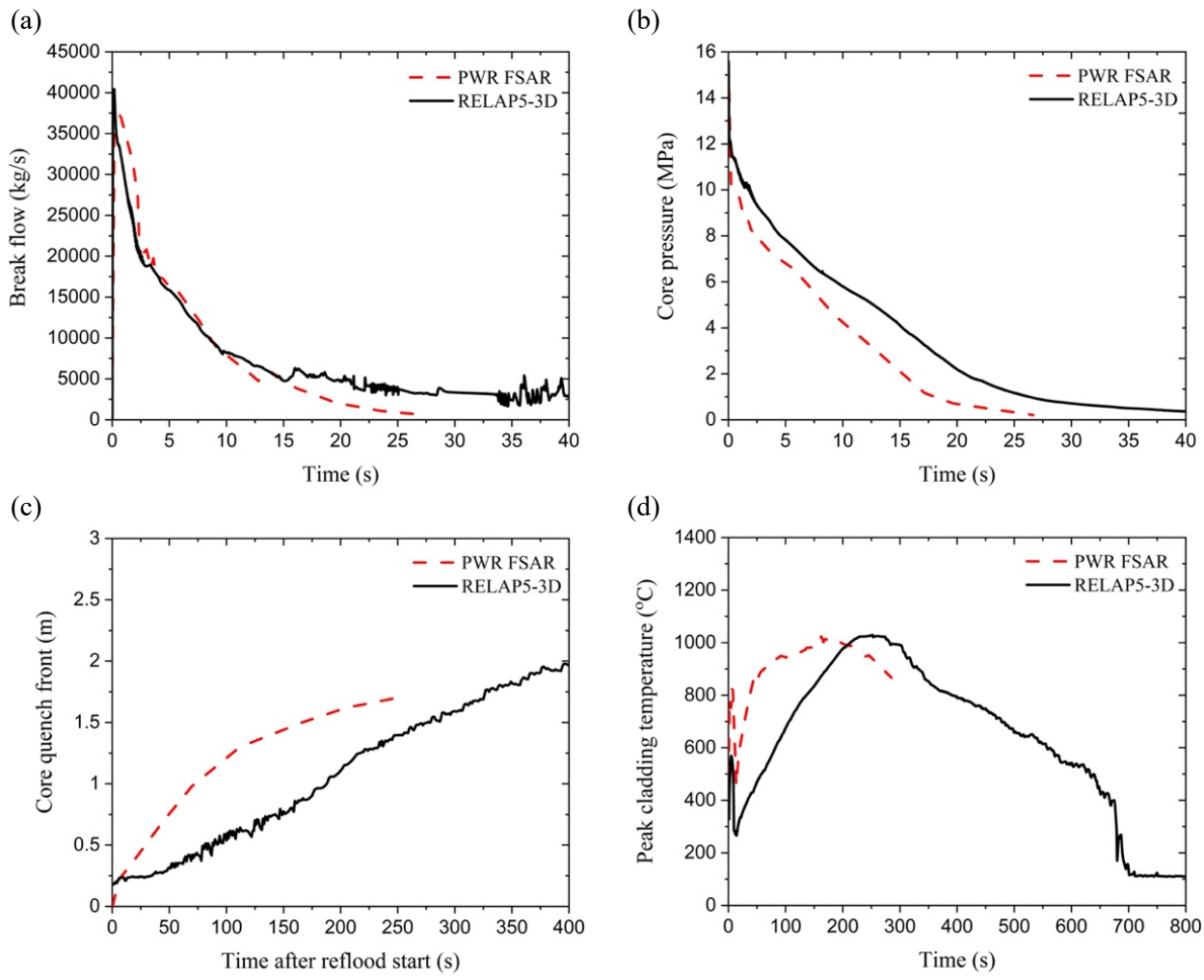

Figure 12. The Vogtle FSAR and representative RELAP5-3D simulation comparisons of (a) break flow, (b) core pressure, (c) core quench front, and (d) peak cladding temperature.

4.2.2 High Burnup LOCA Analysis

Figure 13 shows the G8 high burnup fuel pin EOC steady-state coolant, cladding surface, and fuel temperatures. RELAP5-3D and CTF show axial coolant temperature increase along the long the axial length of the fuel rod, verifying appropriate energy deposition and heat transfer from the fuel rod to the coolant channel. The RELAP5-3D cladding surface temperature results closely agree with the CTF results. Note that VERA models heat transfer enhancement effect downstream of spacer grids, resulting in localized decreases in cladding temperature, causing the jagged effect seen in Figure 13 (b). This effect is not modeled in RELAP5-3D, resulting in a smoother axial temperature profile across the cladding.

BISON and RELAP5-3D fuel centerline temperatures are in excellent agreement. Compared to VERA average fuel temperatures, the RELAP5-3D fuel average temperature is more conservative, as it accounts for the burnup-dependent gap thermal properties (i.e., fission gas thermal conductivity degradation). The same approach and steady-state analysis were conducted for all fuel rods; the results for each case show similar trends as those observed for G8. The comparison of the coolant temperature ensured correct implementation of mass flow rate and power output via the fuel rod. Furthermore, the comparable

cladding surface and fuel centerline temperatures provided ensure that pretransient conditions are consistent in the fuel system conduction calculation.

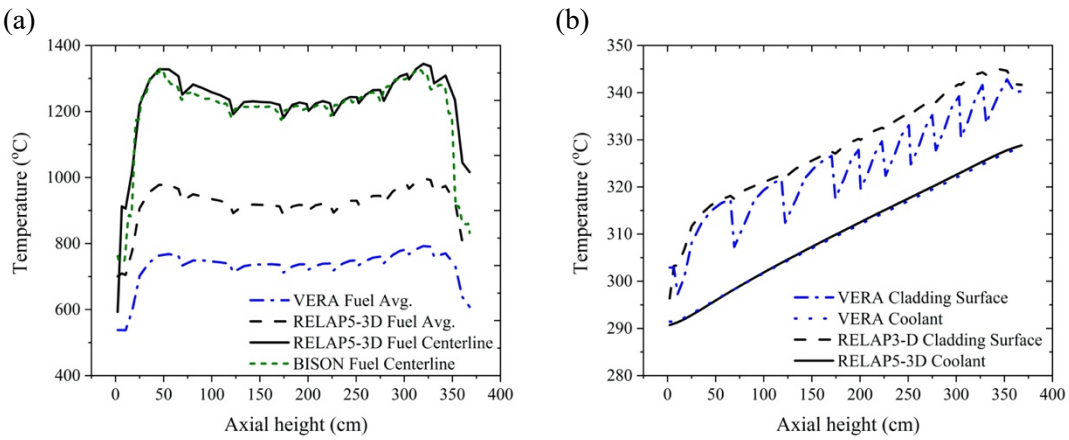

Figure 13. The RELAP5-3D, VERA, and BISON steady-state fuel rod data integration for G8 high burnup fuel pin at the center core: (a) fuel temperature and (b) coolant and cladding surface temperatures.

Following rupture of the cold-leg, the maximum fuel temperature rapidly decreased from the steady-state operating temperature, as seen in Figure 14 (a). Over time, the cladding temperature increases to the PCT reported in Table 3, which reports the peaking factors, PCT, and local burnup for all fuel rods considered. Time-dependent cladding surface heat flux response at the PCT location, as shown in Figure 14 (b), is impacted by heat generation rate, as well as the thermal-hydraulic conditions in the adjacent coolant. During the blowdown and reflood phases, the heat flux rapidly decreases due to the scram-induced decrease in fuel heat generation, and subsequently, the loss of liquid coolant and the decrease in steam flow through the core. The decay heat generated by VERA is applied as a function of time, as shown in Figure 14 (c and d). The applied decay heat sustains the cladding temperature until the quench phase, which occurs at ~600 seconds for the high burnup fuel pin, at which point the heat flux rises due to rewetting and reflood coolant boiling. The heat flux then decreases to ~1.5×10^4 W/m^2 as fuel temperatures stabilize during post-reflood conditions.

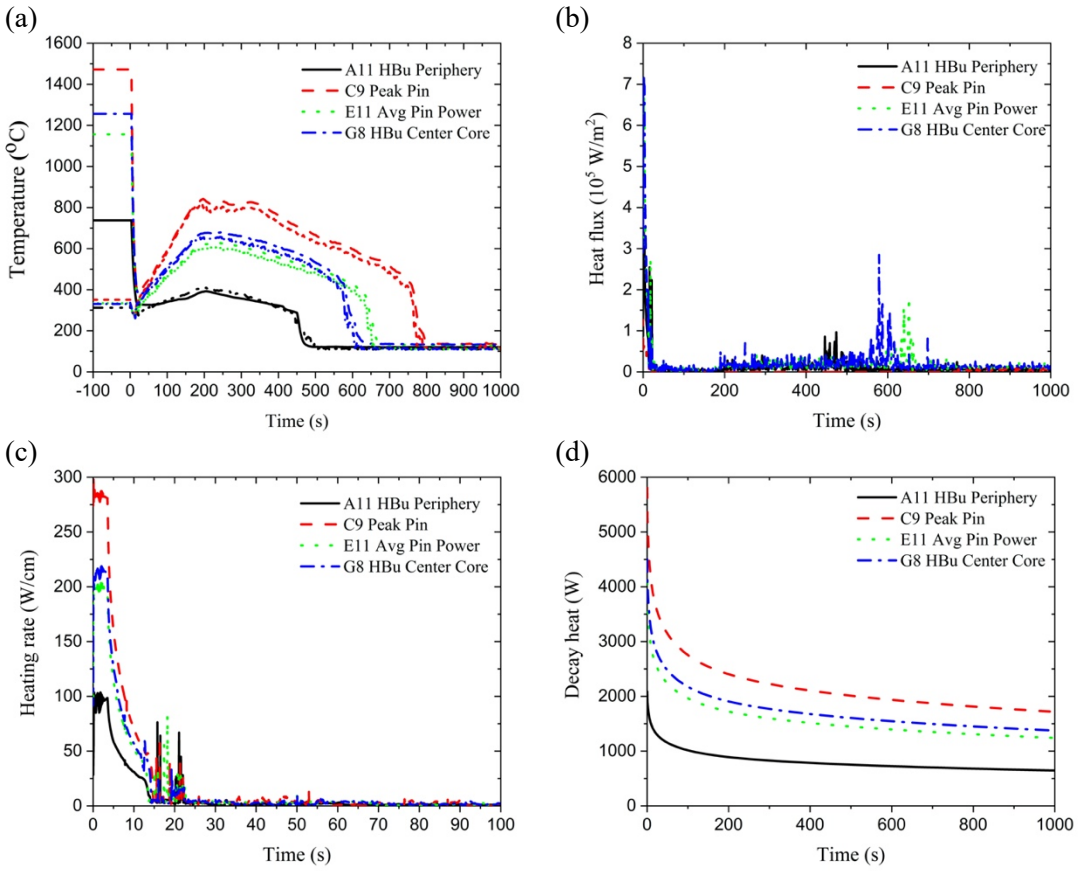

Figure 14. (a) Fuel centerline and cladding surface temperatures, (b) heat flux, (c) heating rate at the PCT location, and (d) decay heat versus time for a LB-LOCA at EOC.

Table 3. Steady-state rod average peaking factor, PCT, and local burnup at PCT location for considered fuel rods.

Assembly fuel rod	Peaking factor	PCT	Local burnup
A11 high burnup core periphery	0.48	410°C	81.1 GWd/MTU
C9 peak temperature pin	1.34	821°C	40.7 GWd/MTU
E11 average pin power	0.94	608°C	71.6 GWd/MTU
G8 high burnup core center	1.04	656°C	75.5 GWd/MTU

4.3 FUEL PERFORMANCE

4.3.1 Steady State Results

4.3.1.1 Operating Conditions

Three fuel rods were identified from the VERA full core depletion analysis for subsequent BISON steady-state and transient analyses. The VERA analysis calculated power and cladding surface temperatures at 98 axial locations. The primary factors for selecting fuel rods were assembly/pin location, rod average burnup, and rod average peaking factor. As a result, two fuel rods from the center of the core and one fuel rod from the periphery of the core were evaluated. One additional fuel rod from assembly C9

was evaluated. This fuel pin had the highest peaking factor, ~1.34, at EOC, with a rod average burnup of 38 GWd/MTU, which resulted in the highest PCT. This fuel rod was intended to serve as a bounding condition for PCT, burst timing, etc. The details of this fuel rod are not listed below since it is not a high burnup fuel rod.

The first fuel rod is Assembly G8 Pin 4-3 (G8). The complete rod average linear heat rating (LHR) for Assembly G8 Pin 4-3 is shown in Figure 15. Assembly G8 was originally located in the F8 position, effectively in an adjacent position. The assembly was moved to G8, directly adjacent to the center assembly, and was surrounded by fresh assemblies. This resulted in the Assembly G8, and more specifically Pin 4-3, operating at high powers for the duration of the cycle, resulting in the highest rod average burnup in the center of the core. The fuel rod accumulated a rod average burnup of 71.56 GWd/MTU during two cycles of operation. Lastly, the dips in the figure are consistent with end-of-cycle refueling outages.

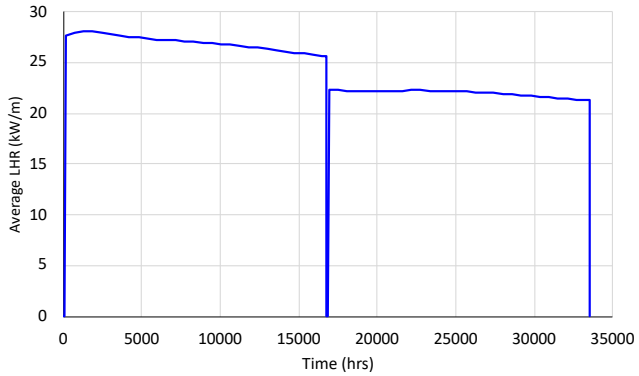

Figure 15. Rod average LHR for fuel rod located in Assembly G8 Pin 4-3.

The second fuel rod was located in Assembly A11 Pin 3-13, and the complete rod average LHR is shown in Figure 16. Assembly A11 was initially located at the L14 position on the ring of fire. Adjacent assemblies were either fresh or twice burned, and as a result, fuel rods adjacent to the fresh fuel assemblies operated at higher power than fuel rods adjacent to the twice-burned assemblies. In particular, Pin 3-13 was located in the assembly region near fresh fuel assemblies. Subsequently, the assembly moved inward, just inside the ring of fire, adjacent to fresh fuel assembles and near once-burned fuel assemblies. Again, Pin 3-13 was regionally located near fresh fuel assemblies, resulting in higher pin powers and additional burnup accumulation as compared to other pins in the assembly. Finally, assembly A11 was moved to the periphery of the core. Pin 3-13 was adjacent to the ring of fire and accumulated the highest rod average burnup in the core at 76.88 GWd/MTU.

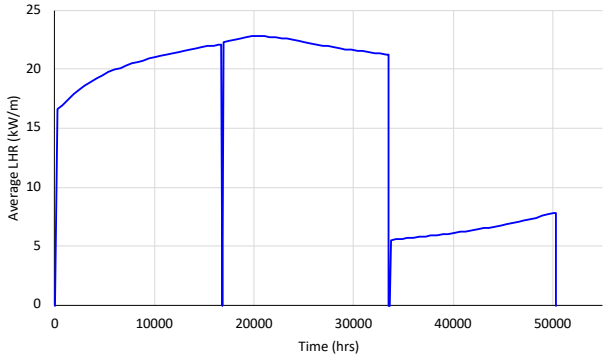

Figure 16. Rod average LHR for fuel rod located in Assembly A11 Pin 3-13.

The final fuel rod was located in Assembly E11 Pin 5-4; Figure 17 illustrates the average LHR for the fuel rod throughout irradiation. Originally, the assembly was located in the ring of fire at D13, where the fuel pin and assembly experienced very high LHRs. The assembly was subsequently moved to E11 and was surrounded by once-burned fuel assemblies. Over time, the average LHR reduced over the course of the cycle. Outside of the fuel rods on the periphery of the core, Assembly E11 had the lowest peaking factors of the high burnup assemblies, accumulating a rod average burnup of 68.8 GWd/MTU.

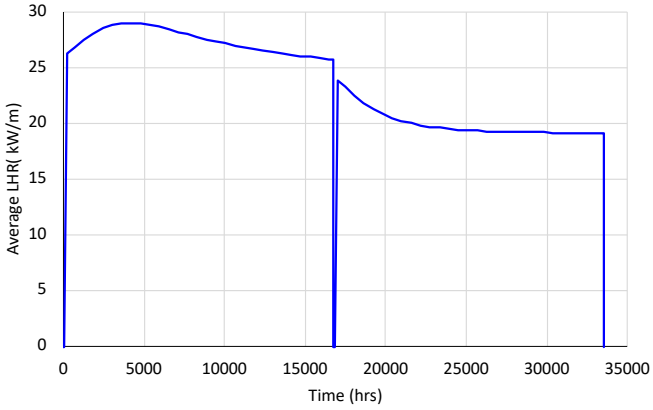

Figure 17. Rod average LHR for fuel rod located in Assembly E11 Pin 5-4.

4.3.1.2 Steady State Analysis Results

Fuel rod evolution during steady-state operation is critical for evaluating fuel performance during LOCA conditions at or near end of life. Furthermore, fundamental fuel performance parameters such as rod internal pressure (RIP) and fuel centerline temperature are important for ensuring that fuel rod integrity is maintained throughout normal operation and anticipated operational occurrences. NUREG-0800, Chapter 4.2, specifically states that RIP should remain below the system pressure and should also account for gas generated though the fission and neutron absorption process [48]. The reviewer guide also states that alternative limits could be provided but must be justified. NUREG-0800, Chapter 4.2, also requires fuel pellet overheating to be evaluated [48]. The reviewer guide states that analyses should be performed for the maximum LHR throughout the core. RIP and fuel centerline temperatures are not only dependent on each other, but they are also highly reliant on fuel rod operating conditions and material models defining fuel rod evolution. Therefore, it is important to evaluate those parameters contributing to evolution of the parameters of interest over the course of operation. Numerous evaluations are likely needed to adequately address the safety case; however, BISON analyses are intended to highlight potential areas of concern or

areas for which additional analyses would provide insightful results. BISON was used to evaluate steady-state performance of each fuel rod prior to the LOCA analysis. Those parameters important to safety were evaluated in order to understand the state of the fuel rod during normal operation. Figure 18 compares rod internal pressure BISON results as a function of time and as-fabricated fuel grain radius. For reference, typical UO_2 fuel grain radii are ~11.5 microns [49]. The BISON results indicate that rod internal pressure could be a serious concern for high burnup fuel rods with smaller grains of 5.75 microns radially. For prototypic grain dimensions, RIP begins approaching the system pressure (~15.5 MPa) and requires more in-depth analyses over a larger range of operating conditions.

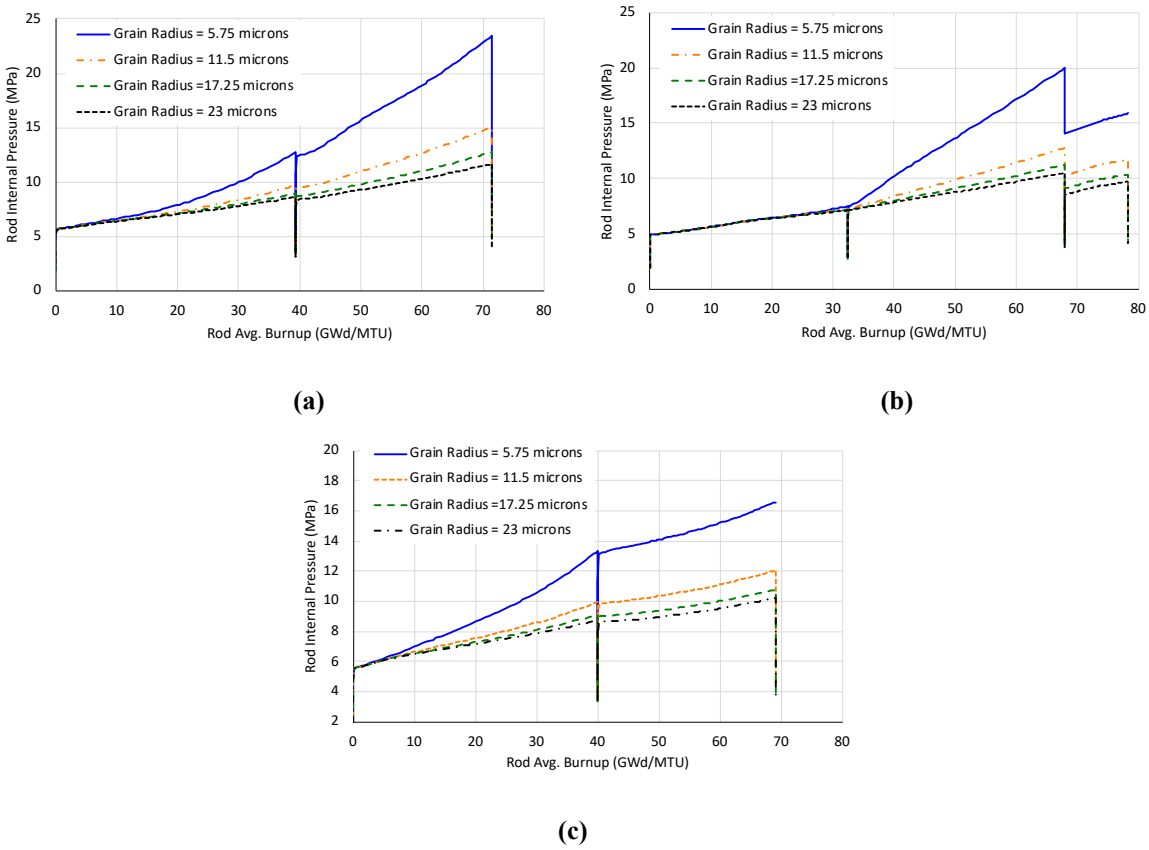

Figure 18. Time-dependent RIP results for (a) G8 Pin 4-3, (b) A11 Pin 3-13, and (c) E11 Pin 5-4.

The impacts of fuel and cladding mechanical changes on RIP are the simplest mechanisms to understand and evaluate. During the irradiation process, UO_2 is subject to a number of phenomena resulting in mechanical deformation (thermal expansion, relocation, swelling, etc.), whereas cladding mechanical changes are primarily driven by irradiation creep. Thermal expansion, elastic deformation, and thermal creep all play secondary roles. Fuel and cladding mechanical changes, with the exception of swelling, impact RIPs early in life, prior to gap closure. Fuel swelling is a constant process resulting from the fission process, when fission products gradually expand the fuel matrix. In the absence of fission, fuel swelling would not occur. Time-dependent fuel and cladding radial strain results are shown in Figure 19. Strain results were taken at the axial location corresponding to the end-of-life peak centerline temperature, (i.e., ~3.13 m from the bottom of the active fuel). As indicated in the figure, fuel and cladding radial strain results for high-powered fuel rods (G8 and E11) converge at ~10 GWd/MTU. This convergence is consistent with pellet-cladding gap closure. Referencing back to Figure 18, RIP for all rods early in life increase at a constant rate while the gap is open. Following gap closure, RIP appears to increase at a faster rate for the high-powered fuel rods (G8 and E11), whereas pin 3-13 in assembly A11

maintains a relatively constant increase in RIP. This constant increase persists until ~32–34 GWd/MTU, at which point the RIP begins to increase at a faster rate.

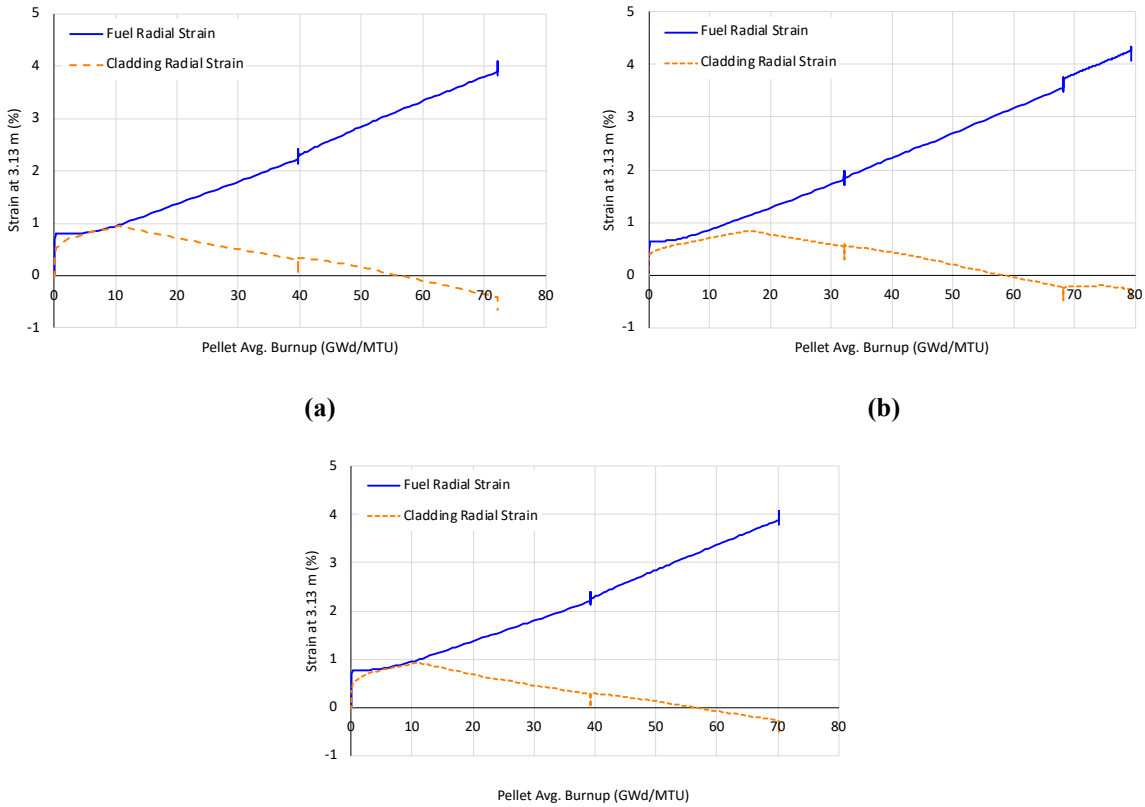

Figure 19. Time-dependent fuel and cladding radial strain results at the axial location 3.13 m from the bottom of the fuel for (a) G8 Pin 4-3, (b) A11 Pin 3-13, and (c) E11 Pin 5-4.

The sudden increase in RIP can be directly correlated to fission gas release (FGR), as seen in Figure 20. Fuel rods in assemblies G8 and E11 operate at very high LHRs, or temperatures, for the majority of operation, resulting in the generation and release of large amounts of fission gas, whereas pin 3-13 in assembly A11 operates at lower LHRs relative to the other analyzed pins. This operating regime delays FGR until fuel temperatures and/or burnup are high enough for fission gas to successfully release into the plenum. Furthermore, improving UO_2 microstructure by increasing the grain size could be a safety benefit and a potential economic benefit as indicated in Figure 18, Figure 20, and Figure 21. Reducing FGR improves the fuel rod's thermal response in high burnup conditions, as shown in Figure 21. RIP and FGR are both decreased by simply increasing the radial size of the grains from 5.75 to 11.5 micrometers. FGR is dependent on fission gas atoms diffusing through the grain to the grain boundary, or free surface, at which point gas atoms are released to the plenum. Increasing the size of the grain increases the diffusion distance, and therefore delays FGR.

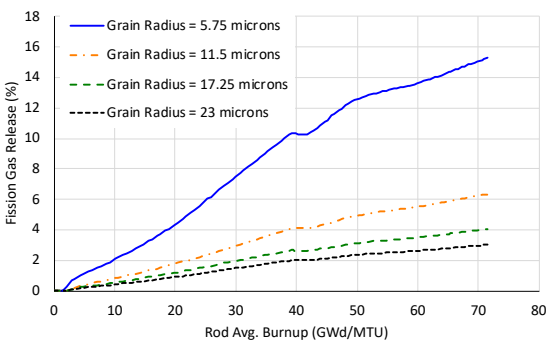

(a)

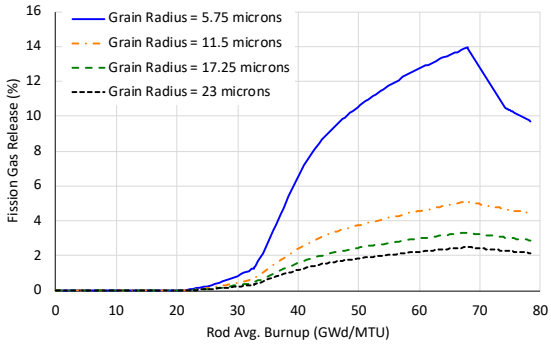

(b)

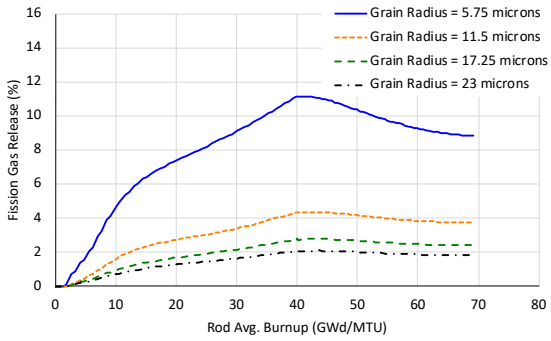

(c)

Figure 20. Time-dependent FGR results for (a) G8 Pin 4-3, (b) A11 Pin 3-13, and (c) E11 Pin 5-4.

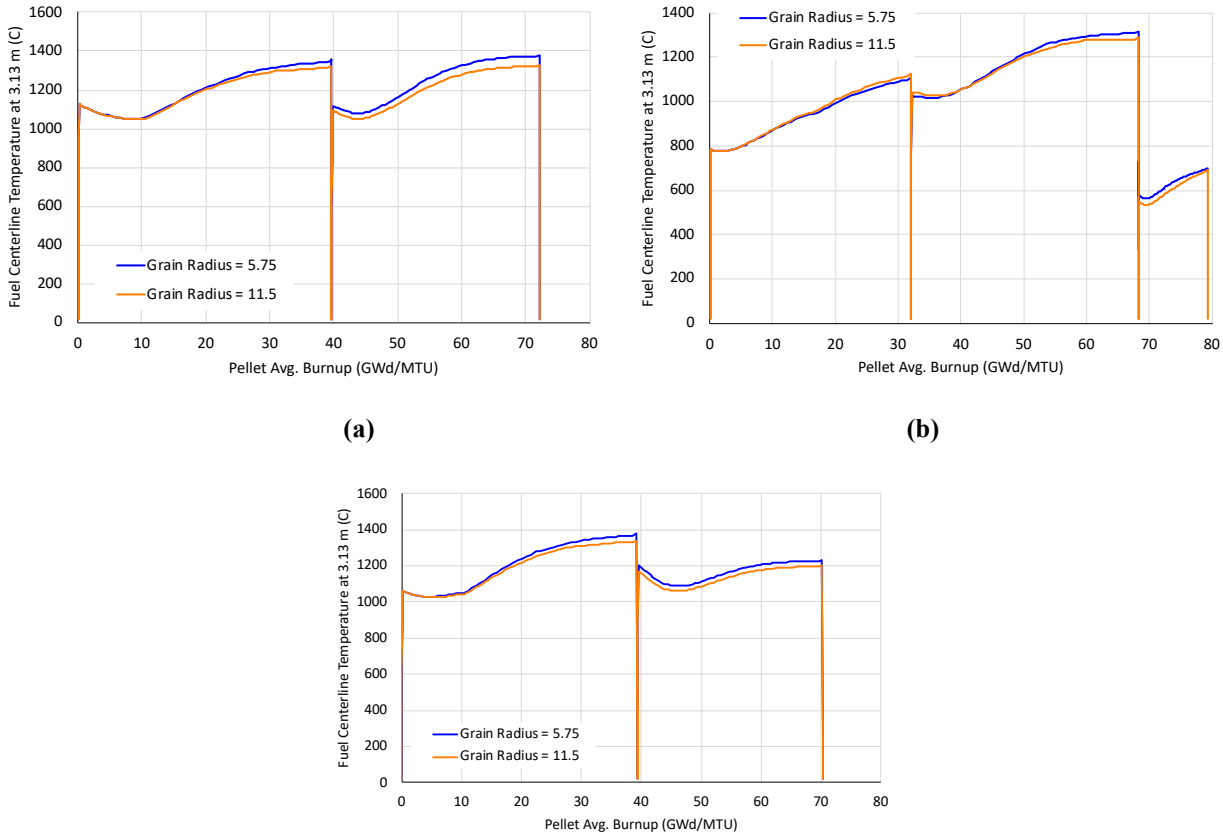

Figure 21. Time-dependent fuel centerline temperature results at the axial location 3.13 m from the bottom of the fuel (a) G8 Pin 4-3, (b) A11 Pin 3-13, and (c) E11 Pin 5-4, indicating lower temperatures with less fission gas.

Released fission gas contaminates thermal conductivity across the gap and further increases fuel temperatures. By reducing FGR, high burnup fuel operates at lower temperatures, thereby improving the high burnup fuel performance and providing additional safety margin to fuel melt during overpower events. However, increasing fuel temperatures and burnup can increase FGR release rates, but this was not observed for larger grain boundaries under the analyzed operating conditions. Operating conditions have a strong impact on FGR, and burnup extension will likely result in more aggressive operating conditions in conjunction with increasing burnup. Therefore, it is important to continue investigating FGR and its impact on fuel performance under high burnup operating conditions.

4.3.1.3 Pre-Transient Fuel Conditions

Currently, mechanisms driving high burnup fuel pulverization and subsequent relocation and dispersal are up for debate. Experimental data to date indicates that fuel pulverization is strongly dependent on local burnup (i.e., nodal burnup and pellet average burnup) and terminal temperature [45]. Experimental conditions to date have used electrically heated or partially electrically heated systems to heat rodlets to LOCA temperatures. At this writing, there has not been an experimental effort designed to replicate pretransient fuel conditions, as well as the evolution of the fuel conditions during a LOCA. One of the key outcomes of this work is to provide experimentalists with prototypic pretransient and transient fuel conditions to support experiments designed to replicate high burnup LOCA conditions observed in

PWRs. It has been hypothesized that the evolution of the fuel pellet stress state during the LOCA contributes to pulverization, so understanding stress evolution across the fuel pellet radius may provide some additional insights to mechanisms contributing to pulverization.

Fuel operating temperatures are among the primary parameters for consideration. Over the course of operation, fuel temperatures across the rod (radially and axially) change as operating conditions evolve. When removing operating conditions and considering a constant power, fuel temperatures initially decrease as the pellet-cladding gap closes. Once gap closure occurs, fuel temperatures continue to increase due to UO_2 thermal conductivity degradation. This occurs until the local pellet burnup exceeds ~60 GWd/MTU, at which time thermal conductivity degradation begins to saturate. However, FGR begins contaminating gap thermal conductivity, and fuel temperatures continue to increase, as seen in Figure 19 through Figure 21. Making the problem more complex, strong fuel temperature and burnup gradians form across the ~4 mm pellet radius, and as a result, local (i.e., center, middle, and rim) regions in the pellet form, with each region containing different microstructural features and mechanical properties.

During normal operation, these burnup and temperature distributions are manageable and do not appear to have detrimental effects. However, a LOCA causes local fuel temperatures to diverge from equilibrium, with the fuel centerline temperature decreasing, and fuel temperature on the periphery increasing, potentially at different rates. Experimentalists trying to replicate LOCA fuel performance must understand prototypic operating conditions (burnup and temperature distribution) to ensure appropriate fuel conditions prior to the LOCA.

Figure 22 highlights local fuel conditions at peak power location prior to the LOCA transient.

Figure 22a illustrates radial fuel temperatures as a function of radial location, while

Figure 22b illustrates radial fuel temperatures as a function of the radial burnup profile. Fuel operating conditions can be divided into two bins and are consistent with the results reported by Zhang et al. [27]. The two bins are associated with the location of the fuel rods in the core: the center of the core and the periphery of the core. VERA results indicate high burnup fuels operating in the center of the core have a rod average peaking factor of ~0.9–1.1 (~17–21 kW/m), and the fuel centerline temperature is expected to range from ~1,000–1,350°C. Operating conditions—radial temperature and burnup—shown in

Figure 22a represent the operating conditions observed in VERA and are comparable to results reported by Zhang et al. [27].

Assembly A11 has the lowest temperature profile, as this fuel rod is located on the periphery of the core, where fuel rods operate at low LHRs with respect to fuel rods in the center of the core. As shown in

Figure 22b and Figure 3, fuel centerline temperatures are below the cladding burst criteria. This indicates that burst may not occur in fuel rods on the periphery of the core, but transient thermal hydraulic and fuel performance analyses are required to confirm. Again, operating conditions observed in this work are consistent with operating conditions identified by Zhang et al. [27], so it is reasonable to assume that the conditions plotted in

Figure 22 can serve as an upper or near upper bound pretransient condition for fuel rods operating on the periphery of the core. It should be noted that these conditions may only be valid for 24-month 4-loop Westinghouse PWRs, as plant operating conditions and cycle lengths could impact fuel operating conditions. However, these results can serve as a reasonable assumption until high burnup core designs

and operating conditions are available for different types of PWRs, as well as for 18-month high burnup fuel cycles.

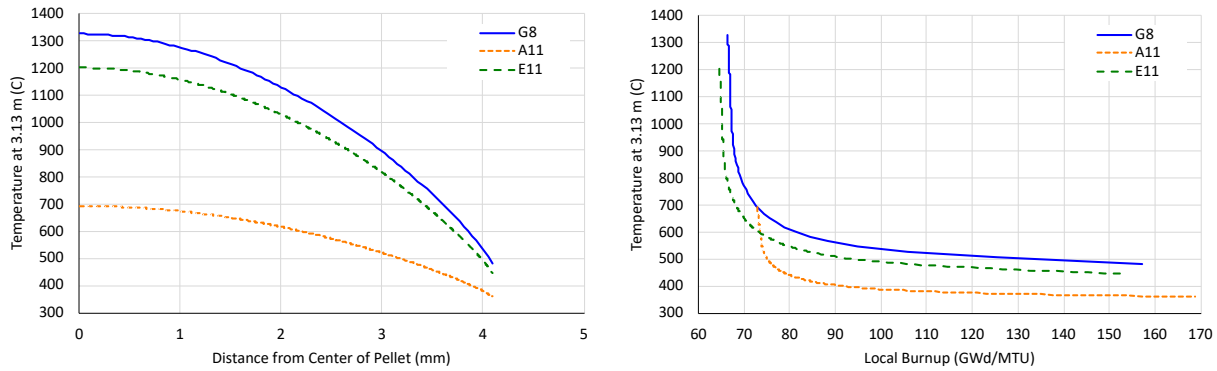

(a) **(b)**

Figure 22. Pre-transient fuel (a) temperature profile as a function of radial position, and (b) temperature profile as a function of radial burnup at the peak power location (~3.13 m from the bottom of the active fuel).

Formation of radial and circumferential cracks in UO_2 has been observed and understood under reactor startup, power changes, and shut down conditions [50–55]. Furthermore, UO_2 cracking has been evaluated using various analysis techniques such as finite element and extended finite element to assess the impact of UO_2 cracking on the overall fuel performance [51–58]. Based on these analyses, it seems reasonable to assume that changes in the fuel pellet stress during a LOCA contributes to pellet pulverization. Figure 23 evaluates pretransient hoop, radial, and axial stresses for the fuel pin from assembly G8. The fuel pellet is under hydrostatic compression. The center of the pellet is in compression, and physically, the center of the pellet is the hottest region, and it thermally expands in all directions more than other regions of the pellet. This thermal expansion behavior results in the cooler regions of the pellet applying compressive stresses on the center region of the pellet. Moving radially toward the pellet periphery, hoop and axial stresses gradually become less compressive and effectively neutral. The expectation would be for tensile stresses to form on the pellet periphery, resulting in cracking of the pellet to reduce stresses. However, cracking is currently not considered; creep is primarily governing the stress state across the pellet. Radial stress is driven by thermal expansion with no external force acting in the radial direction, and therefore, fuel in the radial direction will be in compression throughout the pellet, with the pellet's outer surface being effectively stress free. At the pellet's periphery, hoop and axial stresses become more compressive. This stress transition is a result of pellet-cladding contact. Higher temperatures result in higher axial and hoop tensile stresses on the cladding, and inversely, the cladding imposes compressive stresses on the pellet's periphery.

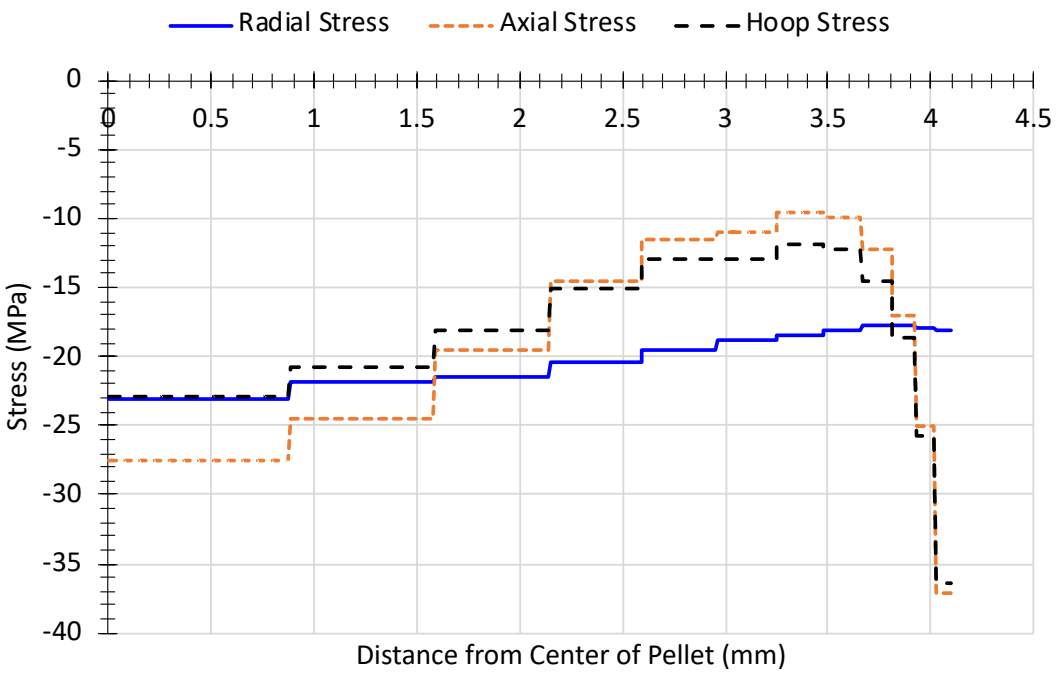

Figure 23. Pretransient hoop, radial, and axial stress profile in the fuel at the peak power location of G8 Pin 4-3.

4.3.2 High Burnup UO_2 Thermal Conductivity Model Comparison

BISON contains a number of UO_2 thermal conductivity models, and recently, new models have been developed using high burnup data. These models are designed to extend BISON's capabilities to higher burnups. To ensure consistency, each model was evaluated and compared to the reference NFIR model, which has been used in both Falcon and BISON. Furthermore, the model has been extensively validated against experimental data up to ~90 GWd/MTU and has been benchmarked to industry codes. Figure 24 compares the fuel centerline temperatures as a function of time for the newly developed models and the NFIR model. Additionally, a porosity correction factor is considered to account for thermal conductivity degradation due to the presence of fission gas bubbles. The porosity correction model does not impact the fuel temperature until late in life (>40 GWd/MTU). However, the fuel centerline temperatures begin to increase rather quickly, leading to an end-of-life temperature difference of ~100°C. This large difference seems to indicate potential double counting at high burnups, as experimental data typically consider the presence of fission gas bubbles. The new models (Ronchi, Staicu, and TopTan) offer vastly different responses. The Ronchi and Staicu models both result in large temperature increases throughout the simulation, whereas the TopTan results are similar to NFIR until the gap closes. Once the gap closes, the TopTan model suggests that fuel temperatures are expected to decrease with respect to the NFIR model. These large differences in temperature with respect to the NFIR model are concerning, as the NFIR model has an extensive history.

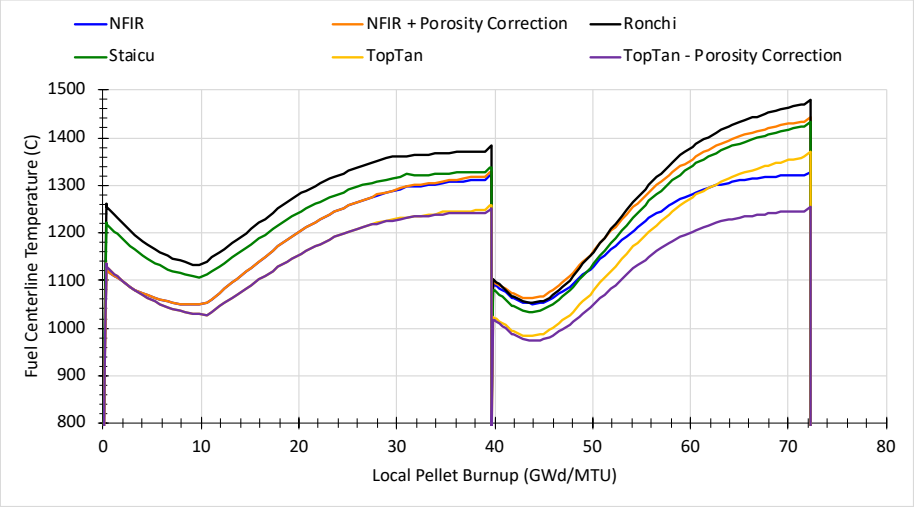

Figure 24. Fuel centerline temperature as a function of time 3.13 m from the bottom of the fuel stack.

Figure 25 evaluates the thermal conductivity at the end-of-life conditions to allow for analysis of these temperature differences. The NFIR model indicates a slight improvement in thermal conductivity moving from the center of the pellet toward the pellet periphery. UO_2 thermal conductivity is temperature dependent, and the expectation is for the thermal conductivity to increase as temperature decreases. At ~3 mm, thermal conductivity degrades rather rapidly, as increasing burnup dominates and degrades thermal conductivity. The other models show similar trends; however, the trends are more drastic in comparison to the NFIR model. The BISON results indicate that the new models needed to be compared to experimental data from the Instrumented Fuel Assembly (IFA) experimental database before being used in commercial application, as the results are inconsistent with the NFIR model. Work moving forward will continue to rely on the NFIR model, which has been used in multiple fuel performance codes and validated up to pellet average burnups of ~90 GWd/MTU.

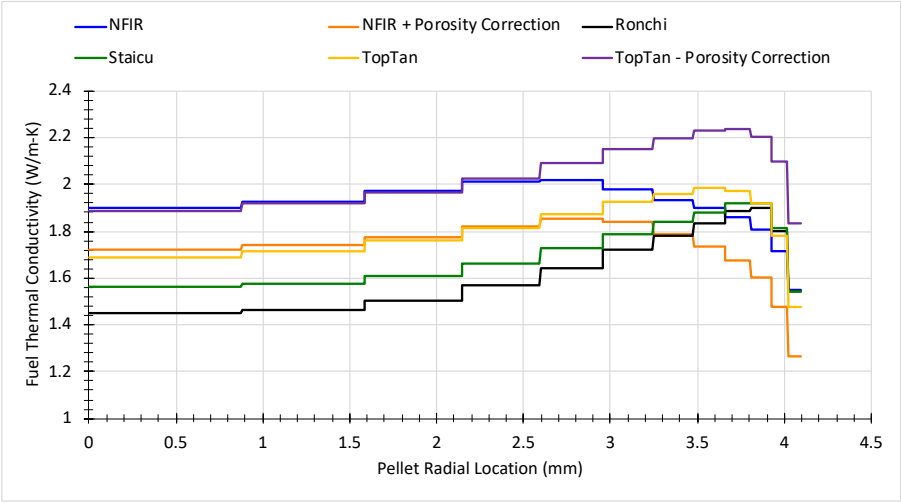

Figure 25. End-of-life UO_2 thermal conductivity as a function of radial location across the fuel pellet.

4.3.3 Transient Results

Cladding burst is the deciding factor for whether or not fuel dispersal occurs during a LOCA. If cladding burst does not occur, then the fuel, even if pulverized, remains in the fuel rod and avoids release. If the

cladding does burst, then fuel dispersal into the reactor coolant system becomes a possibility. The aforementioned fuel rods were evaluated for potential burst under simulated LOCA conditions. Because neither of the high-burnup fuel rods reached the temperatures and stress conditions necessary to burst, an additional once-burned fuel pin from assembly C9 was evaluated.

Cladding burst was evaluated by comparing burst temperature calculated from Eq. (1). The cladding is assumed to have burst when the cladding temperature and stress conditions align with Eq. (1). Figure 26 compares C9 Pin 7-10 cladding temperature and hoop stress at the burst location to the burst criteria. In this case, burst occurs once the cladding temperature reaches 790°C, which is higher than the reported high burnup LOCA integral test [8–12]. High burnup LOCA tests indicated that cladding burst occurs between ~675–750°C. There are reported burst tests in which the cladding did not burst until the temperatures observed in the BISON simulation were reached. However, pretransient rod internal pressures for these experiments were significantly less, whereas the pretransient rod internal pressure was near the system pressure of ~12.3 MPa. Burst test on full length rods may be worth investigating this discrepancy, however, the current model is built on more conservative data.

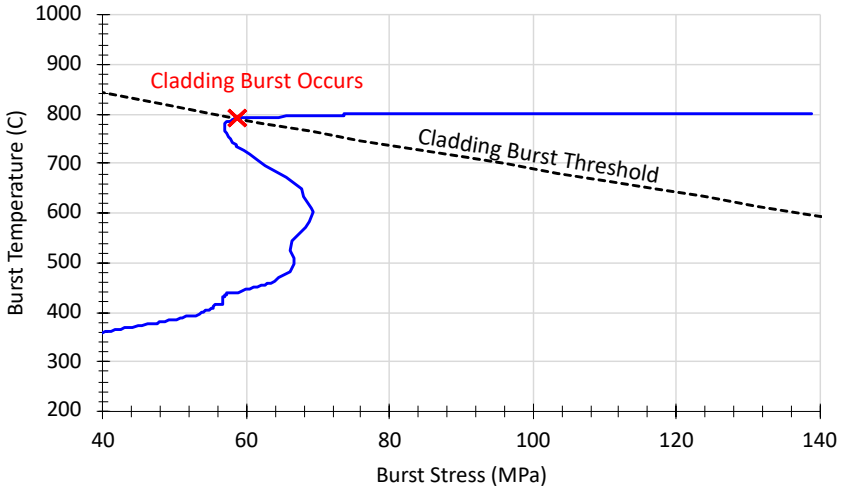

Figure 26. Burst temperature as a function of burst stress for C9 Pin 7-10 (peak temperature rod).

Rodlets used in integral LOCA experiments and cladding burst test use similar cladding radii and thicknesses, but individual rodlets are typically 0.3 m long. Commercial fuel rods, however, are significantly longer (~3.6 m) than these rodlets (0.3 m). Because commercial fuel rods have a much larger internal volume than test rodlets, rod internal pressure decreases at a faster rate as a balloon forms. This sustained pressure allows ballooning to occur axially along the cladding, with increased deformation corresponding to higher temperatures. Fuel rod temperatures uniformly increase until the reflood process begins quenching the fuel rod from bottom to top. As the reflood process progresses, local axial regions of the fuel rod cool, terminating the local ballooning process. This results in subsequently smaller changes to the fuel rod's internal volume and pressure conditions. Consequently, upper spans of the cladding tube are subject to increased temperatures for a longer period of time, allowing larger balloon sizes to form, and increasing the likelihood of burst.

Figure 27 shows cladding hoop strain and temperature as a function of axial location along the fuel rod at the time burst occurs. Due to higher temperatures, there is noticeably more cladding deformation, and burst occurs in the upper regions of the fuel rod. Hoop strain depressions are located near spacer grids and/or mixing vanes which serve as a structural member, stabilizing the fuel rods. Cladding temperatures in these regions are noticeably less. Localized lower temperatures result in localized decreases in cladding

hoop strain during the LOCA. It should be noted that mixing vanes and spacer grids were not explicitly modeled in BISON, but they were included in VERA to generate steady-state conditions (cladding temperature, axial power, etc.) used in these simulations. Effectively, the neutronic and thermal hydraulic effects of spacer grids are included, but the structural features like constraint are not. These results are expected to change by including the structural restraint of spacer grids and associated conditions during the LOCA; the addition of a mechanical constraint will lead to deeper depressions along the hoop strain profile.

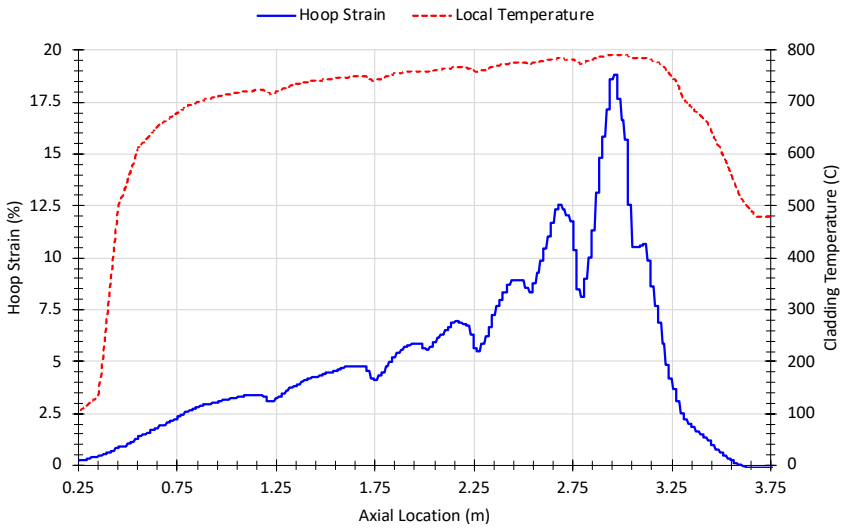

Figure 27. Hoop strain and cladding temperature profile as a function of axial location at the time burst occurred for C9 Pin 7-10 (hot rod).

Peak hoop strain and axial lengths of the cladding balloon are consistent with experimental observations [3,5,6-13]. Figure 28 provides a comparison of cladding burst temperature as a function of hoop strain for a variety of cladding burst test experiments, and Figure 29 shows the axial cladding hoop strain profile of rodlet 192 from the NRC LOCA test program. The peak hoop strain indicates that cladding failure would have been likely to occur for these cladding temperatures at nearly the same time by assessing a strain-based failure criterion instead of the burst temperature model used in this simulation. The peak hoop strain observed for this simulation is ~19% at a temperature of nearly 790°C, consistent with experimental results shown in the figure. The balloon length calculated from BISON is consistent with the length between spacer grids, ~22.8–25.4 cm, while Figure 29 indicates the balloon length is between ~10–15 cm. BISON simulation results are conservative with respect to the LOCA test, but explicitly modeling the spacer grids may improve the accuracy of balloon length calculations.

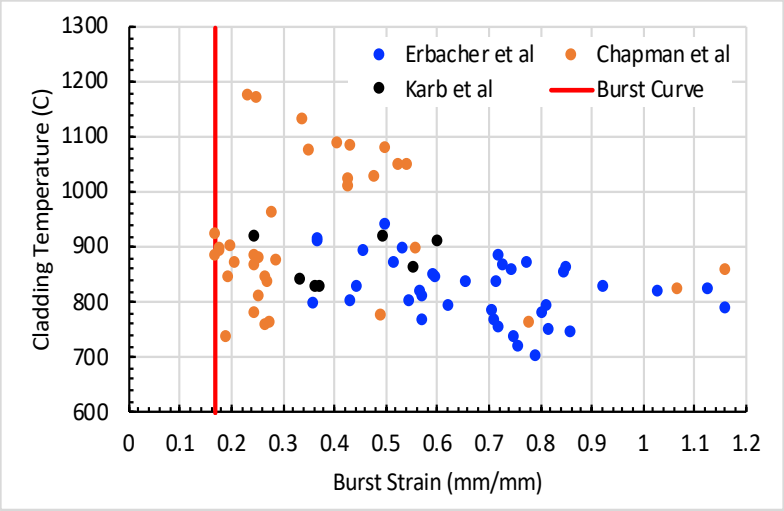

Figure 28. Experimental peak hoop strain data generated through various cladding burst test programs [6,7,59].

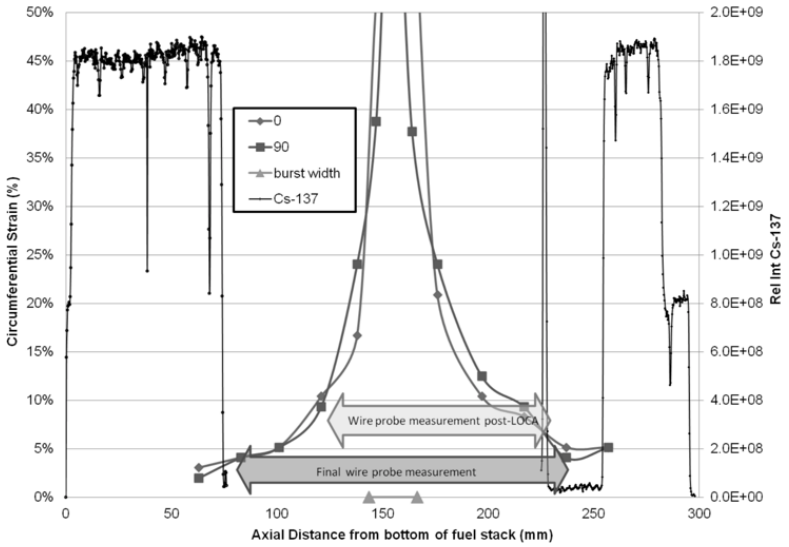

Figure 29. Hoop strain distribution and post LOCA fuel loss measurements as a function of axial location for NRC LOCA rodlet 192 [11,12].

The size of the burst opening may impact the amount of fuel susceptible to dispersal from the cladding. Therefore, it is important to estimate the size of the burst opening by correlating the size of the cladding balloon to the burst opening. Figure 30 shows experimental data used to develop a correlation between the length of burst length to balloon hoop strain (Figure 30a) and between burst length and burst width (Figure 30b). Scatter in the data makes it difficult to determine a conservative length, so two correlations were considered. The first correlation is an upper bound as a function of hoop strain and is driven by the FR-2 data. The second is correlated to the high burnup LOCA integral test data. BISON predicts a peak hoop strain of ~19%. Mapping this strain to the correlations seen in Figure 30a indicates that the burst length is expected to range from 0–6.5 mm. Burst width data (Fig. 23b) show a clear correlation to burst length. Mapping a conservative burst length of 6.5 mm to Figure 30b indicates that the expected width of the burst opening is ~3 mm. This would indicate that the area of the burst is ~19.5 mm^2. Considering the area of a fuel pellet from the side is ~82 mm^2, the burst opening is ~23% the size of a fuel pellet. Fuel dispersal has primarily been experimentally observed and not measured, but the observations indicate that

fuel dispersal becomes significant once the area of the burst opening is larger than the fuel pellet [8–13]. Experimental observations indicate that small amounts of pulverized fuel disperse when the area of the burst opening is less than the area of a pellet. However, it is not possible at this time to quantify the amount dispersed from the opening.

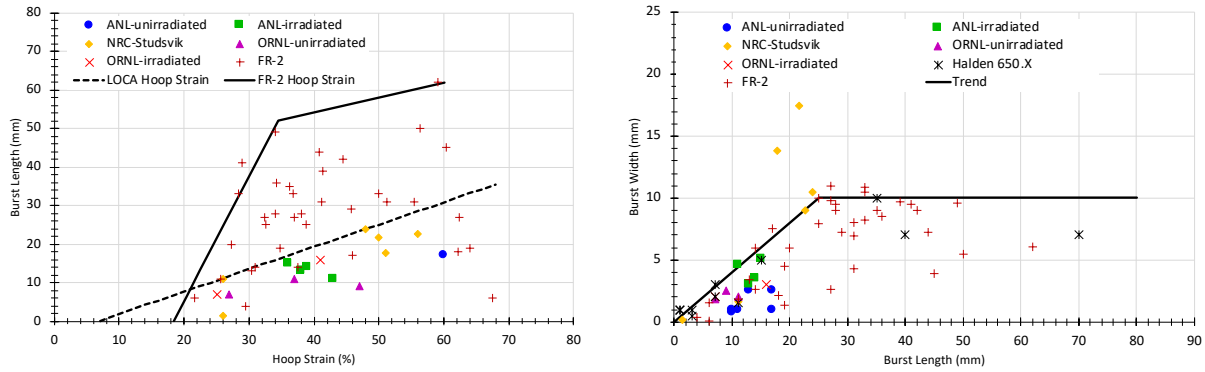

(a) **(b)**

Figure 30. Burst (a) length and (b) width correlation to the peak hoop strain observed in LOCA test programs [8–13,60,61].

4.3.4 Fuel Susceptibility to HBFF

Determining fuel susceptibility to HBFF requires knowing the pellet average burnup and terminal, hottest temperature at the burst location. Radial burnup and temperature profiles can then be mapped to the Turnbull pulverization model to calculate the depth of fuel which may pulverize. The thermal hydraulic analysis indicated that burst would occur in the region near the peak power, which, for high burnup fuel rods, occurs at ~2.7 m from the bottom of the fuel. Figure 31 shows the average fuel pellet burnup distribution at the expected burst location for every rod exceeding a rod average burnup of 62 GWd/MTU. The bulk of the pellet burnup ranges from 70–72 GWd/MTU, with the highest burnup being 77 GWd/MTU. It should be noted that the burnups listed below are rounded up to the nearest burnup for conservatism.

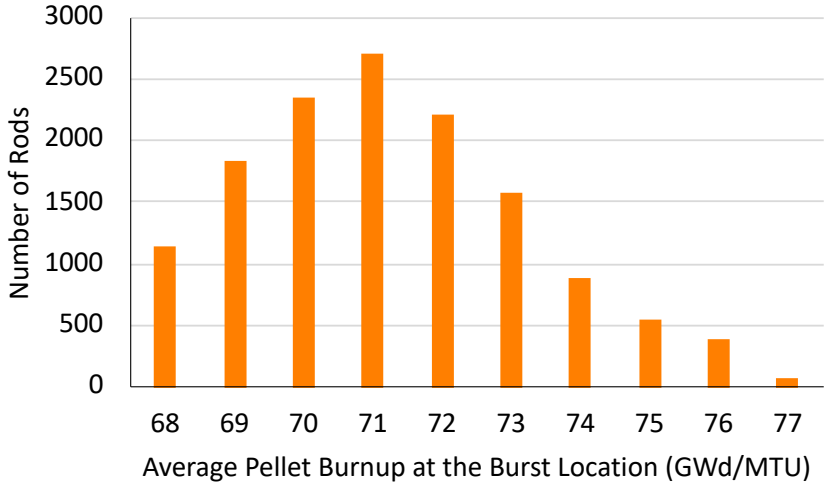

Figure 31. Pellet average burnup distribution at the burst location for every rod that exceeded a rod average burnup of 62 GWd/MTU.

Fuel temperatures were calculated and used to determine pulverization susceptibility. Figure 32 shows the calculated percentage of fuel susceptible to pulverization for average fuel pellet burnups ranging from 63 to 77 MWd/kgU. Two temperatures were considered: 656 and 821°C. 656°C is consistent with the expected PCT for high burnup fuel rods in the center of the core. Additional high burnup fuel rods were modeled in RELAP5-3D, and the results indicated that lower temperatures would be observed, as well. Higher temperatures may occur as every rod was not evaluated, so a bounding case was developed using the highest power fuel rod at EOC (C9). The PCT for this fuel rod was 821°C. This temperature will serve as a bounding temperature, as it is likely one of the hottest rods in the core. Fuel susceptibility to pulverization between the two fuel temperatures range from 1–16% susceptibility; 1% susceptibility is assumed to account for pulverization occurring in the pellet rim region. Pulverization may not occur in this region. However, to conservatively estimate the amount of fuel pulverized, it is assumed that at least 1% of the pellet will be susceptible to pulverization for all burnups and temperatures observed. The worst case scenario observed is 16%, which occurs only in the highest temperatures and at pellet average burnups > 73 GWd/MTU.

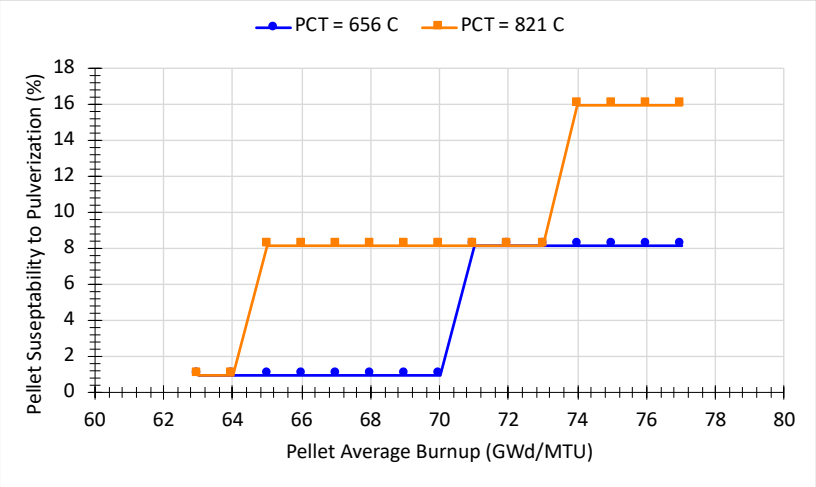

Figure 32. Percentage of fuel pellet susceptible to pulverization in percent for the best estimate and core-wide PCT over the burnup range of interest.

Coupling the cladding response discussed in the previous section to the results in Figure 32 allows for calculation of fuel pulverization susceptibility throughout the core. BISON and integral LOCA experimental results determine the burst length, which influences the length of fuel susceptible to pulverization. The NRC LOCA data suggest that the susceptibility region ranged from 10.16–15.24 cm, or 4–6 inches, whereas BISON indicates that the susceptibility region spans between spacer grids at 24.94 cm, or 9.8 inches. Again, BISON results are expected to overpredict fuel pulverization susceptibility compared to the experimental results. The total fuel volume susceptible to pulverization can be calculated by multiplying the susceptible cross sectional area by the axial length of 10–25 cm. Susceptible fuel mass is calculated by multiplying the total susceptible fuel volume by the density of UO_2. It should be noted that fuel susceptibility does not indicate the occurrence of HBFF; it simply means that the local burnup and temperature conditions exceeded the prescribed threshold and may experience HBFF.

Table 4 summarizes the results. The BISON best estimate analysis indicates that 106.4 kg of fuel will be susceptible to pulverization; when accounting for uncertainties and assuming the worst-case scenario, this value increases to 182 kg. However, experimental data suggest that the length of the cladding balloon is expected to be smaller than that predicted by BISON, so the amount of mass susceptible to pulverization is expected to decrease, as well. Another implication not considered is the impact of delayed burst. Burst was not predicted to occur in any of the high burnup fuel rods. Burst only occurred for the once-burned

fuel rod near the PCT of 790°C. Experimental data indicate that hydrostatic pressure can reduce pulverization susceptibility by ~40%. However, additional experimental data are needed to investigate the implications on the fuel rod level. The fact still remains that delaying burst until higher temperatures are reached will likely decrease the amount of fuel susceptible to pulverization. However, it is not possible to quantify this effect at this time.

Table 4. Full core estimation of HBFF susceptibility

Assumed segment length (cm)	PCT = 656°C (kg)	PCT = 821°C (kg)
10.16[+]	43.3	74.4
15.24[+]	65	111.6
24.94[*]	106.4	182.6

[+]NRC LOCA experimental susceptibility region
[*]BISON predicted susceptibility region

4.3.5 Fuel Pellet Conditions during a LOCA

The previous section describes pretransient fuel conditions, but analyses targeting the fuel mechanical evolution during a LOCA are sparse. Figure 33 illustrates the radial temperature profile time history during a LOCA, and Figure 34 illustrates a radial stress (radial, axial, and hoop) distribution as a function of time during a LOCA. Fuel temperatures decrease from steady-state temperatures to the coolant temperatures with in ~5 seconds, as shown in Figure 33. During the blowdown period, thermal hydraulic conditions are such that the coolant can effectively extract heat from the fuel. The fuel does not start heating up until the blowdown is complete, and as the fuel temperatures begin to rise, the temperature profile is effectively flat. This is consistent with fuel temperatures calculated in the literature [4] and is related to the characteristic time for heat produced in the UO_2 to be removed. Effectively, in the absence of fission, decay heat can be removed from the system, assuming a constant heat sink, within 5–10 seconds. This changes slightly with increasing fuel burnup; so, the fuel is expected to have a flat temperature profile during the LOCA heat-up phase, regardless of the fuel burnup.

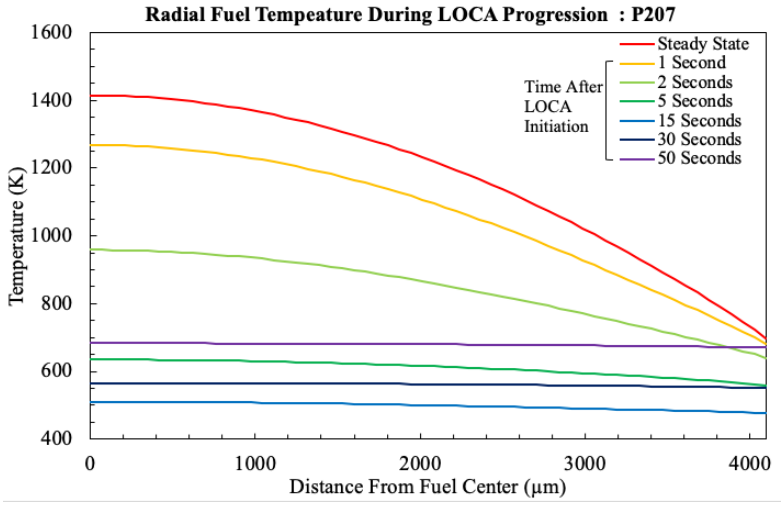

Figure 33. Radial temperature evolution of prior to and during LOCA.

Figure 34 indicates that a LOCA has adverse effects on the fuel pellet stress state. As discussed above, the radial stress profile under steady-state operation is in equilibrium. Stress relaxation in the fuel occurs through a combination of plastic deformation (i.e., creep, plastic flow, hot pressing) occurring in the center of the pellet and crack formation on the pellet periphery. During a LOCA, the temperature profiles of the fuel pellet changes dramatically, causing stresses to form and become more severe as the LOCA progresses. BISON LOCA results indicate that the center of the pellet experiences significantly high tensile stresses above the unirradiated UO_2 fracture stress (~120–200 MPa); the pellet periphery experiences excessively high compressive stresses in the hoop and axial direction. These results indicate that the center of the pellet would form tensile cracks in the radial and circumferential direction, while the pellet periphery may experience compressive failure. However, these results do not indicate whether the stresses would persist following crack formation; nor do they indicate how many cracks are needed to alleviate the stress.

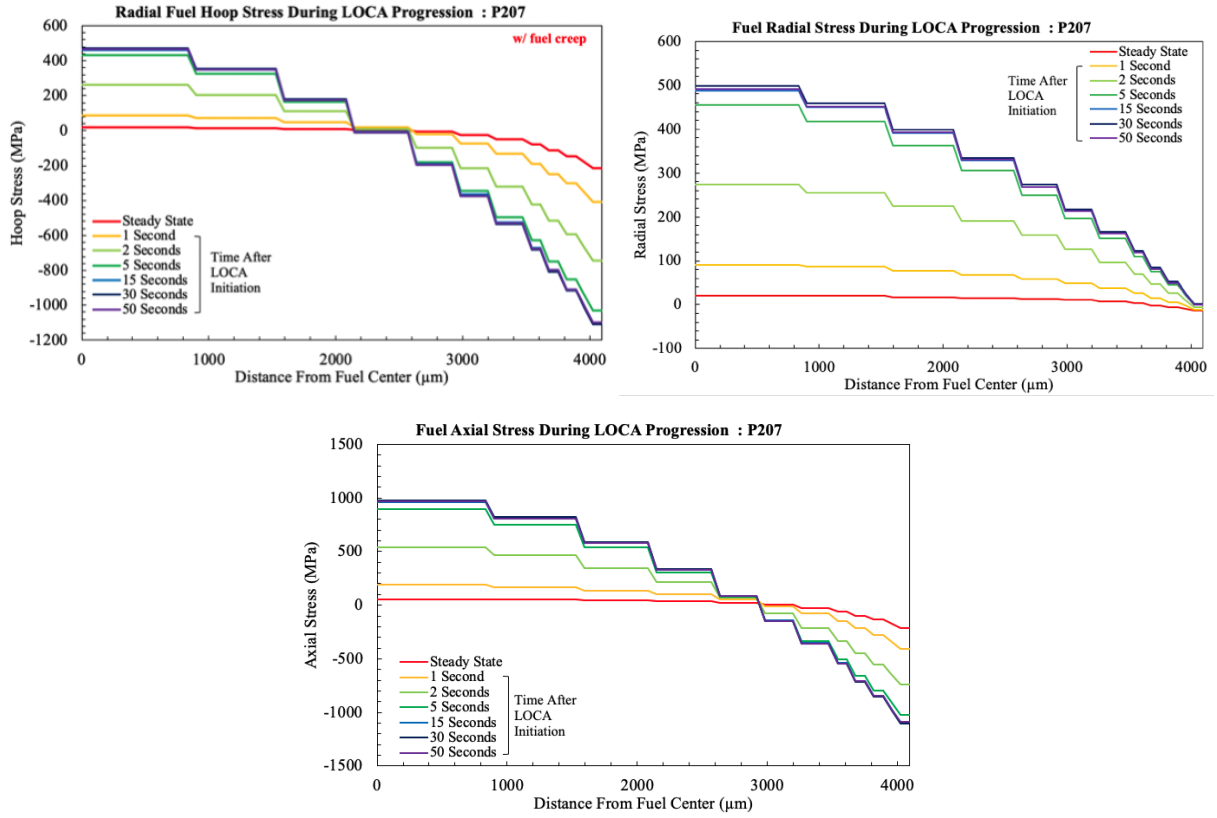

Figure 34. Radial (a) hoop stress, (b) radial stress, and (c) axial stress evolution prior to and during LOCA.

BISON results clearly indicate the relationship between pretransient operating conditions and transient stress formation. Pretransient operating conditions define the equilibrium state of the fuel, and that equilibrium state is contingent on the temperature gradient. As fuel conditions diverge from equilibrium, stresses naturally form until relieved by some mechanism. However, mechanisms governing stress relaxation in UO_2 only occur in fission environments and at high temperatures of >700°C. Once power is removed and fuel temperatures decrease below ~700°C, creep (irradiation and thermal) is inactive, so the fuel stress state will remain unchanged, irrespective of time. Pellet cracking has been observed in previously irradiated fuel and is expected. However, these results suggest that additional, potentially extensive cracking above that previously observed is expected. The implication of these results clearly indicates that LOCA transients can be replicated by knowing the rodlet's pretransient operating

conditions (i.e., rodlet power history) and uniformly heating the rodlet under representative heating rates with an electrical furnace or nuclear heating systems. Effectively, fuel conditions are set post irradiation, and if the temperature profile is flat and heating rates are prototypic, then the heating method is irrelevant. To confirm, two rodlets with similar pretransient operating conditions and average burnups would need to be identified: one rodlet would be sent to Oak Ridge National Laboratory's Severe Accident Test facility, and the other to INL TREAT for LOCA testing.

5. CONCLUSIONS

Results from a full-core LOCA analysis for a core containing high burnup fuel are described herein. VERA was used to deplete a 24-month equilibrium high burnup core design. RELAP5-3D performed a transient thermal hydraulic evaluation of a select few high-impact high burnup fuel rods, and BISON evaluated the steady-state and transient fuel rod response to determine fuel susceptibility to pulverization. The objective of this work was to investigate fuel susceptibility, as well as conditions that lead to fuel susceptibility, to fuel fragmentation, relocation, and dispersal for a realistic case. A secondary objective was to identify prototypic LOCA conditions in order to support accelerated integral LOCA testing.

VERA results identified the location and operating conditions of high burnup fuel rods throughout the core. These conditions were found to be in line with high burnup depletion analyses. Best-estimate thermal hydraulic analyses indicated that high burnup fuel would experience PCTs of ~656°C. Additionally, thermal hydraulic analysis was performed on a once-burned fuel rod, with the highest EOC LHR serving as a bounding condition. The thermal hydraulic analysis results were consistent with the literature. BISON evaluated fuel rod performance prior to and during a LOCA. These results were used to calculate the total amount of fuel susceptible to pulverization throughout the core. The analysis was performed for best estimate as well as for the highest temperature observed in the core. Best estimate BISON results coupled with RELAP TH results identified cladding burst in full length commercial fuel rods are likely to occur at higher temperatures than burst conditions observed in twelve-inch cladding burst test. BISON did not predict cladding burst in high burnup fuel rods, and as a result, cladding burst results for the highest power fuel rod was used to calculate the size of the cladding balloon. BISON results indicated that 106kg of fuel will be susceptible to pulverization, while experimental cladding balloon data suggest 43-65kg of fuel will pulverize. In an attempt to quantify the worst-case scenario, BISON evaluated pulverization susceptibility in high burnup fuel rods using the RELAP cladding temperature for the highest power fuel rod in the core. The results indicated 182kg of fuel would pulverize.

Finally, fuel pellet temperature and stress conditions were calculated prior to the LOCA transient and during the transient. BISON indicated fuel temperatures during the blowdown phase decrease to the coolant temperature and are flat. Fuel temperatures during the refill phase increase uniformly at rate consistent with the cladding thermal boundary conditions; decay heat had negligible impact on fuel temperatures. Fuel stress conditions across the pellet prior to the LOCA range from +/- 50 MPa. These stress conditions are developed in the presence of a temperature gradient and are in equilibrium prior to the transient. Reactor shutdown removes this temperature gradient resulting in stresses forming across the pellet radius. In the absence of fission and below ~700°C, stress relaxation would not occur, and therefore, the resultant stresses induced by the reactor shutdown, or scram, would not change, irrespective of time after shutdown, unless pellet cracking occurred. At the onset of LOCA, fuel stresses continue to diverge from the equilibrium stress conditions as the flat temperature profile increases to the point where tensile and compressive cracks are expected to form in the center of the pellet and on the pellet periphery. This behavior indicates UO_2 performance under LOCA conditions is reliant on pre-transient operating conditions conditioning the fuel pellet prior to the LOCA and the impact of decay heat would have no impact on pellet fracture or pulverization. The evidence clearly suggests that LOCA fuel behavior will be

identical under integral nuclear heated and electrically heated LOCA experiments provided the pre-transient power, rodlet average burnup, and heating rate are similar. Future work should consider replicating in-pile and furnace experimental conditions using commercial fuel irradiated under similar burnup and pre-transient power conditions to support the BISON conclusions.

6. ACKNOWLEDGMENTS

The effort to develop 24-month cycle design for the included analysis would not be possible without the collaboration of SNC. Nuclear Energy Advanced Modeling and Simulation Program (NEAMS) of the US Department of Energy Office of Nuclear Energy supported the fuel analysis, while the Consortium for Advanced Simulation of Light Water Reactors (CASL, www.casl.gov) VERA Users Group funded capability development and supported SNC efforts. The authors would like to express appreciation to Jordan Rader and Ian Greenquist of the ORNL Reactor and Nuclear Systems Division for their support in the review of this manuscript. Furthermore, Southern Nuclear Company contributions cannot be understated, as they provided representative core designs, industry expertise, and overall vision for how NEAMS can support the industry through strategic modeling and simulation evaluations. Lastly, this research made use of the resources of the High Performance Computing Center at Idaho National Laboratory, which is supported by the Office of Nuclear Energy of the U.S. Department of Energy and the Nuclear Science User Facilities under Contract No. DE-AC07-05ID14517.

7. REFERENCES

1. Burns, J.R., Hernandez, R., Terrani, K.A., Nelson, A.T. and Brown, N.R., 2020. Reactor and fuel cycle performance of light water reactor fuel with 235U enrichments above 5%. *Annals of Nuclear Energy*, *142*, p.107423.
2. *Standard Review Plan for the Review of Safety Analysis Reports for Nuclear Power Plants: LWR Edition – Transient and Accident Analysis*, NUREG-0900, Chapter 15.
3. F. Erbacher and S. Leistikow, "Zircaloy Fuel Cladding Behavior in a Loss-of-Coolant Accident: A Review," in *Zirconium in the Nuclear Industry*, eds. R. Adamson and L. S. Van (West Conshohocken, PA: ASTM International, 1987), 451–488.
4. K.A. Terrani, D. Wang, L.J. Ott, R.O. Montgomery, "The Effect of Fuel Thermal Conductivity on the Behavior of LWR Cores during Loss-of-Coolant Accidents," *J. Nucl. Mater.* 448 (2014). doi:10.1016/j.jnucmat.2013.09.051.
5. M. Billone, Y. Yan, T. Burtseva, R. Daum, *Cladding Embrittlement During Postulated Loss-of-Coolant Accidents*, NUREG/CR-6967, U.S. NRC, Office of Nuclear Regulatory Research, 2008.
6. F. J. Erbacher, S. Leistikow, *A Review of Zircaloy Fuel Cladding Behavior in a Loss-of-Coolant Accident*, KfK 3973, Kernforschungszentrum Karlsruhe Germany, 1985.
7. F. J. Erbacher, H. J. Neitzel, K. Wiehr, *Cladding Deformation and Emergency Core Cooling of a Pressurized Water Reactor in a LOCA*. Summary Description of the REBEKA Program. Scientific Report KfK 4781, Karlsruhe (1990)
8. W. Wiesenack, *Summary of the Halden Project LOCA Test Series IFA-650*, HPR-380, OECD NEA Halden Reactor Project, May 2013.
9. L. Lekkonen, *LOCA Testing in Halden, the Fourth Experiment: IFA-650.4*, HWR-838, OECD Halden Reactor Project, January 2007.
10. B.C. Oberlander, M. Espeland and N. O Solum, "PIE Results from the High Burnup (92 GWd/MTU) PWR Segment after LOCA Testing in IFA 650-4," *Proc. of the EHPG Meeting*, Sandefjord 2011.

11. P. A. C. Raynaud, “Fuel Fragmentation, Relocation, and Dispersal during Loss-of-Coolant Accidents,” US NRC, Office of Nuclear Regulatory and Research, NUREG-2121, March 2012.

12. M. Flanagan, P. Askeljung, A. Purana, *Post-Test Examination Results from Integral High Burnup Fueled LOCA Test at Studsvik Nuclear Laboratory*, US NRC, Office of Nuclear Regulatory and Research, NUREG-2160, August 2013.

13. P. Askeljung, J. Flygare, and D. Minghetti, “NRC LOCA Testing Program at Studsvik, Recent Results on High Burnup Fuel,” *Proc. 2012 Top Fuel Conf.*, Manchester, United Kingdom, September 2–6, 2012.

14. K. Une, S. Kashibe, and A. Takagi, “Fission Gas Release Behavior from High Burnup UO_2 Fuel at Rapid Heating Conditions,” *Proc. 2005 Water Reactor Fuel Performance Meeting*, Oct 3–6 2005.

15. “Report on Fuel Fragmentation, Relocation, Dispersal,” Nuclear Energy Agency, Committee on the Safety of Nuclear Installations, NEA/CSNI/R(2016)16,October 2016.

16. E Kolstad et al., “High Burnup Fuel Behavior under LOCA Conditions as Observed in Halden Experiments: Fuel Behavior and Modelling under Severe Transient and Loss of Coolant Accident (LOCA) Conditions.” *Proceedings of a Technical Meeting*, Mito, Japan, 18–21 October 2011. IAEA-TECDOC-CD-1709.

17. J. Noirot et al., “Size and Radial Origin of Fragments Formed while Heating a 83 GWd/tU PWR Fuel up to 1200°C,” Minutes of the HRP-WGFS Workshop on Fuel Fragmentation, Relocation and Dispersal, Aix en Provence May 2015, by Wolfgang Wiesenack. HWR-1147, July 2015.

18. M. Bruet et al., “High Burn-Up Fuel Behaviour during a LOCA Type Accident: the FLASH 5 Experiment,” IAEA Technical Committee Meeting on Behavior of Core Materials and Fission Product Release in Accident Conditions in LWRs, Cadarache, France, 1992.

19. Y. Yan, , Burns, Z. M., Smith, T. S., Linton, K. D., Yueh, K., Terrani, K. A. *LOCA Fragmentation Test with High Burnup HBR Fuel Rod*. United States: N. p., 2020.

20. K. Govers and M. Verwerft. “Simulation of Ballooning and Relocation in the Halden LOCA Tests with FRAPTRAN.” in EHPG meeting 2014. Røros.

21. G. Khvostov, A. Romano, M.A. Zimmerman, “Modeling the Effects of Axial Fuel Relocation in the IFA-650.4 LOCA Test,” in Enlarged Halden Programme Group Meeting 200711–16 March 2007: Storefjell Hotel, Gol, Norway.

22. Y. Tofino, A. Concejal, P.J. Garcia Sedano. Evaluation of ECR and PCT in balloon region under LOCA conditions of the Halden IFA 650 tests (single rod tests). in TopFuel. 2009. Paris.

23. C. Grandjean, G. Hache. “LOCA Issues Related to Ballooning, Relocation, Flow Blockage and Coolability,” in *SEGFSM Topical Meeting on LOCA Issues*. 25–26 May 2004 ANL.

24. J. Karlsson, P. Beccau, P. Magnusson, C. Janzon, C. Struzik, M. Dostal, I. Porter, L. Jernkvist, G. Grandi, C. Jönsson, W. Zheng, T. Taurines, S. Belon, O. Marchand, X. Shuo, H.-U. Zwicky, Modelling Out-of-Pile LOCA Tests on High Burnup Fuel Rods.” Results of the Fourth SCIP Modelling Workshop (2018).

25. K. A. Gamble, “Axial Relocation Model Extension in Bison.” United States: N. p., 2018. Web. DOI:10.2172/1605203.

26. R. L. Williamson et al., Tech. Rep. CASL-U-2019-1856-000, Consortium for Advanced Simulation of Light Water Reactors, May 2019.

27. H. Zhang, C. Blakely, J. Yu, R. Stewart, M. Asgari, "Fuel Rod Burst Potential Evaluation under LOCA Conditions for an Existing Plant with Extended Burnup Exceeding the Current Limit by 20%," INL/EXT-19-55888, September 2019.

28. B. Kochunas, B. Collins, S. Stimpson, R. Salko, D. Jabaay, A. Graham, Y. Liu, K. S. Kim, W. Wieselquist, A. Godfrey, K. Clarno, S. Palmtag, T. Downar, J. Gehin, "VERA Core Simulator Methodology for Pressurized Water Reactor Cycle Depletion," *Nuclear Science and Engineering*, 185:1, 217–231, DOI: 10.13182/NSE16-39, 2017.

29. A. Godfrey, B. Collins, K.S. Kim, R. Montgomery, J. Powers, R. Salko, S. Stimpson, W. Wieselquist, K. Clarno, J. Gehin, S. Palmtag, R. Montgomery, D. Jabaay, B. Kochunas, T. Downar, N. Capps, J. Secker. *VERA Benchmarking Results for Watts Bar Nuclear Plant Unit 1 Cycles 1–12*. United States: N. p., 2016.

30. A. Godfrey, B. Collins, C. Gentry, S. Stimpson, J. Ritchie, *Watts Bar Unit 2 Startup Results with VERA*. United States: N. p., 2017. Web. doi:10.2172/1355891.

31. D. Salazar, F. Franceschini, P. Petrarca, A. Godfrey, S. Stimpson, T. Evans, B. Collins, C. Gentry,. AP1000 PWR Cycle 1 HFP Depletion Simulations with VERA. United States: N. p., 2016.

32. B. Collins, S. Stimpson, B. W. Kelley, M. T. H. Young, B. Kochunas, E. W. Larsen, T. Downar, A. Godfrey, "Stability and Accuracy of 3D Neutron Transport Simulations Using the 2D/1D Method in MPACT," *J. Comp. Phys.* 326, 612, 2016.

33. K. Kim, M. Williams, D. Wiarda, A. Godfrey, "Development of a New 47-group Library for the CASL Neutronics Simulator," *Proc. ANS MC2015—Joint International Conference on Mathematics and Computation (M&C), Supercomputing in Nuclear Applications (SNA) and the Monte Carlo (MC) Method*, April 19–23, 2015, Nashville, Tennessee, 2015.

34. R. Salko, T. Lange, V. Kucukboyaci, Y. Sung, S. Palmtag, J. Gehin, M. Avramova, "Development of COBRA-TF for Modeling Full-Core, Reactor Operating Cycles," *Advances in Nuclear Fuel Management V* (ANFM 2015), March 29–April 1, Hilton Head, South Carolina, 2015.

35. I. Gauld, G. Radulescu, G. Ilas, B. Murphy, M. Williams, D. Wiarda, "Isotopic Depletion and Decay Methods and Analysis Capabilities in SCALE," *Nucl. Technol.* 174(2), 169, 2011.

36. B. Rearden, M. Jessee, Eds., *SCALE Code System*, ORNL/TM-2005/39, Version 6.2, Oak Ridge National Laboratory, Oak Ridge, Tennessee, 2016. Available from Radiation Safety Information Computational Center as CCC-834.

37. D. Gaston, C. Newman, G. Hansen, D. Lebrun-Grandie. "MOOSE: A Parallel Computational Framework for Coupled Systems of Nonlinear Equations" *Nucl. Eng. Des.* 239: 1,768, 2009.

38. R. L. Williamson, N. A. Capps, W. Liu, et al. "Multi-Dimensional Simulation of LWR Fuel Behavior in the BISON Fuel Performance Code," JOM 68, 2016.

39. Southern Nuclear Operating Company, Inc., *Vogtle Electric Generating Plant Unit 1 and Unit 2 - The Final Safety Analysis Report*, 1997.

40. American Nuclear Society, ANSI/ANS-5.1-1979, *Decay Heat Power in Light Water Reactors*, August 1989.

41. J. Ikeda, E. Kolstad, *In-Pile Determination of Thermal Conductivity of Oxide Layer on LWR Cladding*. Technical Report NFIR III RPX-103-04, February 1996.

42. C. M. Allison, G. A. Berna, R. Chambers, E. W. Coryell, K. L. Davis, D. L. Hagrman, D. T. Hagrman, N. L. Hampton, J. K. Hohorst, R. E. Mason, M. L. McComas, K. A. McNeil, R. L. Miller, C. S. Olsen, G. A. Reymann, L. J. Siefken, SCDAP/RELAP5/MOD3.1 Code Manual, Volume IV:

MATPRO–A Library of Materials Properties for Light-Water-Reactor Accident Analysis. Technical Report, NUREG/CR-6150, EGG-2720, Idaho National Engineering Laboratory, 1993.

43. N. Capps et al., "Development and Demonstration of a Methodology to Evaluate High Burnup Fuel Susceptibility to Pulverization under a Loss of Coolant Transient," *Nuclear Engineering and Design*, under review, 2020.
44. R. Chapman. Multirod Burst Test Program: Progress Report. Oak Ridge, Tennessee; Springfield, Virginia, Dept. of Energy, Oak Ridge National Laboratory, US Nuclear Regulatory Commission, 1978.
45. J. Turnbull et al.. "An Assessment of the Fuel Pulverization during LOCA-Type Temperature Transients, *Nucl. Sci. Eng.* 179, 1–5, 2015.
46. C. M. Allison, G. A. Berna, R. Chambers, E. W. Coryell, K. L. Davis, D. L. Hagrman, D. T. Hagrman, N. L. Hampton, J. K. Hohorst, R. E. Mason, M. L. McComas, K. A. McNeil, R. L. Miller, C. S. Olsen, G. A. Reymann, L. J. Siefken, "SCDAP/RELAP5/MOD3.1 Code Manual, Volume IV: MATPRO–A Library of Materials Properties for Light-Water-Reactor Accident Analysis." Technical Report, NUREG/CR-6150, EGG-2720, Idaho National Engineering Laboratory, 1993.
47. P. G. Lucuta, H. J. Matzke, I. J. Hastings, "A Pragmatic Approach to Modelling Thermal Conductivity of Irradiated UO_2 Fuel: Review and Recommendations. *Journal of Nuclear Materials*, 232(2–3):166–180, 1996.
48. *Standard Review Plan for the Review of Safety Analysis Reports for Nuclear Power Plants: LWR Edition* (NUREG-0800) United States Nuclear Regulatory Commission, ML042080088.
49. "Effect of Startup Ramp Rate on Pellet-Cladding Interaction of PWR Fuel Rods" EPRI Technical Report TR-112140-V2, April 1999.
50. Y. Aleshin, C. Beard, G. Mangham, D. Mitchell, E. Malek, M. Young, "The Effect of Pellet and Local Power Variations on PCI Margin," Proceedings of Top Fuel 2010, September 26-29, Orlando, FL, USA, Paper 041, 2010.
51. N. Capps, A. Mai, M. Kennard, W. Liu, "PCI analysis of Zircaloy Coated Clad under LWR Steady State and Reactor Startup Operations Using BISON Fuel Performance Code," *Nuclear Engineering and Design* 332, pp. 383–391, 2018.
52. N. Capps, S. Stimpson, K. Clarno, B. D. Wirth, and J. Rashid, "Assessment of the Analysis Capability for Core-Wide PWR Pellet-Clad Interaction Screening of Watts Bar Unit 1," *Nuclear Engineering and Design*, Volume 333, pp. 131–144, 2018.
53. N. Capps, M. Kennard, W. Liu, B. D. Wirth, J. Rashid, "PCI Analysis of a Commercial PWR Using BISON Fuel Performance Code," *Nuclear Engineering and Design*, Volume 324, pp. 131–142, 2017.
54. N. Capps, R. Montgomery, D. Sunderland, M. Pytel, and B. D. Wirth, "Evaluation of Missing Pellet Surface Geometry on Cladding Stress Distribution and Magnitude," *Nuclear Engineering and Design*, Volume 305, pp. 51–63, 2016.
55. Z. Zhang, W. Jiang, J. E. Dolbow, et al. "A Modified Moment-Fitted Integration Scheme for X-FEM Applications with History-Dependent Material Data. *Comput Mech* **62,** 233–252, 2018. https://doi.org/10.1007/s00466-018-1544-2
56. W. Jiang, B. W. Spencer, J. E. Dolbow, "Ceramic Nuclear Fuel Fracture Modeling with the Extended Finite Element Method," *Engineering Fracture Mechanics*, Volume 223, 106713, ISSN 0013-7944, 2020.
57. *Fuel Reliability Guidelines: Pellet-Cladding Interaction* EPRI Technical Report 1015453, December 2008.

58. *PCI Analyses and Startup Ramp Rate Recommendations for Westinghouse Fuel in Exelon PWRs* EPRI Technical Report 1012915, April 2006.

59. R. Chapman, *Multirod Burst Test Program: Progress Report.* Oak Ridge, Tennessee; Springfield, Virginia, Dept. of Energy, Oak Ridge National Laboratory, US Nuclear Regulatory Commission, 1978.

60. E.H. Karb et al., "KfK in-Pile Tests on LWR Fuel Rod Behavior During the Heatup Phase of a LOCA," KfK-3028, ISSN 0303-4003, October 1980.

61. E.H. Karb et al., "LWR Fuel Rod Behavior in the FR2 In-Pile Tests Simulating the Heatup Phase of a LOCA," KfK-3346, ISSN 0303-4003, March 1983.